Aus dem
Helmholtz Zentrum München
Comprehensive Pneumology Center (CPC)

Specialized fibroblasts in wound healing

Dissertation
zum Erwerb des Doctor of Philosophy (Ph.D.) an der Medizinischen Fakultät der Ludwig-Maximilians-Universität München

vorgelegt von
Bikram Dasgupta

aus
Kolkata / Indien

Jahr
2024

Mit Genehmigung der Medizinischen Fakultät der
Ludwig-Maximilians-Universität München

Erstes Gutachten:	Prof. Dr. Jürgen Behr
Zweites Gutachten:	Dr. Yuval Rinkevich
Drittes Gutachten:	Priv. Doz. Dr. Andreas Ohlmann
Viertes Gutachten:	Prof. Dr. Daniela Hartmann

Dekan: Prof. Dr. med. Thomas Gudermann

Tag der mündlichen Prüfung: 01.08.2024

LMU LUDWIG-MAXIMILIANS-UNIVERSITÄT MÜNCHEN

Promotionsbüro
Medizinische Fakultät

MMRS

Affidavit

Dasgupta, Bikram

Surname, first name

Max-Lebsche-Platz 31

Street

81377, Munich, Germany

Zip code, town, country

I hereby declare that the submitted thesis entitled:

Specialized fibroblasts in wound healing

is my own work. I have only used the sources indicated and have not made unauthorized use of the services of a third party. Where the work of others has been quoted or reproduced, the source is always given.

I further declare that the dissertation presented here has not been submitted in the same or similar form to any other institution for the purpose of obtaining an academic degree.

Munich, 14.08.2024 — place, date

Bikram Dasgupta — Signature doctoral candidate

LMU LUDWIG-MAXIMILIANS-UNIVERSITÄT MÜNCHEN

Promotionsbüro
Medizinische Fakultät

MMRS

Confirmation of congruency between printed and electronic version of the doctoral thesis

Dasgupta, Bikram

Surname, first name

Max-Lebsche-Platz 31

Street

81377, Munich, Germany

Zip code, town, country

I hereby declare that the submitted thesis entitled:

Specialized fibroblasts in wound healing

is congruent with the printed version both in content and format.

Munich, 14.08.2024

place, date

Bikram Dasgupta

Signature doctoral candidate

Contents

Abbreviations 6

Summary 7

Introduction 9

Introduction to Mammalian Wound Repair 9

Regeneration vs Scarring 10

Fibroblasts 13

Specialized fibroblasts in Wound Healing 15

Migration dynamics 17

A map of fibroblast states in wound healing 18

Results 20

Skin wounds contain diverse fibroblasts 20

Differentiation capacity of CD201^{+} cells 22

Impaired CD201^{+} progenitor differentiation blocks wound healing 26

Permissive differentiation checkpoints in wound fibroblasts 29

Instructive checkpoint of fibroblast differentiation 33

Translation in human physiology 38

Discussion 41

Material and methods 44

List of Tables 66

List of Figures 67

Contribution to the figures 69

Acknowledgements 70

Abbreviations

α-SMA	α-smooth muscle actin
Akt	Protein kinase B
CNS	Central Nervous system
ECM	Extra cellular matrix
EGF	Epidermal growth factor
EMT	Epithelial-to-mesenchymal transition
En-1	Engrailed 1
EPF	Engrailed-1 transcription factor positive fibroblast
FGF	Fibroblast growth factor
GFP	Green fluorescent protein
Hif1α	Hypoxia-inducible factor 1-alpha
IL-1ß	Interleukin 1 beta
MBNL1	Muscleblind-like1
MRTF	Myocardin-related transcription factor
mTOR	Mammalian target of rapamycin
NHS	N-Hydroxysuccinimide
NSC	Neural Stem cells
TGF	Transforming growth factor
TNF	Tumor necrosis factor
PI3K	Phosphoinositide 3-kinase
PAGA	Partition-based graph abstraction
Pro-Hyp	Prolyl hydroxypropyl
RA	Retinoic Acid
SCAD	Scar on a dish
UMAP	Uniform manifold approximation and projection
WBR	Whole body regeneration

Summary

Connective tissue fibroblasts are the primary cell type influencing and choreographing wound healing outcomes. We have previously identified a diversity of fibroblast cell types, of which one such population termed EPFs (Engrailed-lineage positive fibroblasts) undergo collective cell migration towards the center of the wound to generate scars (Jiang et al., 2020). The EPF cell lineage inhabits all layers of skin connective tissue (papillary, reticular, hypodermal, fascia), highlighting the need for a deeper understanding of the anatomic origins and differentiation trajectories of this pro-scarring fibroblast subset during wound healing stages.

In this study, we aimed to investigate the mechanisms underlying skin tissue healing by examining the coordination of swelling, contraction, and scar formation. We focused on a specific group of fibroblast progenitor cells that express CD201 exclusively in fascia, which is the innermost layer of connective tissue in the skin.

To understand the role of these $CD201^+$ progenitor cells in wound healing, we conducted a study using scRNAseq, murine skin injury models, gene ablation and genetic lineage tracing systems to explore and identify all stromal cells and pinpoint the scar-forming subset, at single-cell resolution. Through these approaches, we were able to demonstrate that these $CD201^+$ progenitor cells are crucial in regulating the pace of healing wounds. We found that these $CD201^+$ progenitor cells give rise to different specialized cell types in a carefully orchestrated differentiation sequence, including inflammatory, proto- and myofibroblasts. Importantly, we discovered that the activation of retinoic acid and hypoxia signaling pathways serves as the initial triggers for the sequential transition of these progenitor cells into proinflammatory and myofibroblast states, thereby pacing wound healing phases. By manipulating the differentiation of $CD201^+$ progenitor cells, we were able to disrupt the spatiotemporal development of fibroblasts and significantly delay the healing process in wounds. Thus, we outlined the process of fascia progenitor-to-myofibroblast transition and identified key checkpoints and their regulators involved in the healing course post-injury. This highlights the key role of $CD201^+$ fascia progenitors in wound healing.

Overall, our study provides valuable insights into the role of $CD201^+$ progenitor cells in wound healing and offers a way to chart the basic biology of fibroblast responses during wound repair.

Such findings are highly medically relevant, as shifts in differentiation might compromise wound healing and lead to pathological scarring disorders such as fibrotic scarring, desmoplastic reactions in tumor development, scar contractures, hypertrophic scars, and keloids as well as delayed wound healing outcomes as seen in diabetes and aging. Modulating $CD201^{+}$ fascia progenitors may open new avenues to alter the function of the fibroblasts that could achieve positive outcomes for enhanced wound repair across a range of pertinent medical settings.

Introduction

Introduction to Mammalian Wound Repair

Mammalian wound repair is a highly regulated process that involves various phases & cellular responses that aim to restore tissue integrity and function following injury (Cordeiro and Jacinto, 2013; McCarty et al., 2012; Ryu et al., 2019). These phases and responses work together to restore tissue integrity and function after an injury (Cañedo-Dorantes and Cañedo-Ayala, 2019). During this process, various cellular and molecular events occur in a well-orchestrated manner to ensure proper healing (Abdellah et al., 2019). An important result of mammalian healing repair is the formation of fibrotic scars, which occur in most wound-healing cases (Arno et al., 2014). Scarring is characterized when components like collagen, fibronectin, proteoglycans and other matrix fibrillary macromolecules are excessively deposited in the tissue upon wounding and subsequently impair the normal course of healing of wounds resulting in several pathological diseases. The clinic is grappling with the burden of scarring, a significant issue that affects both patients and society. Current strategies often require long and painful treatments, which may still yield sub-optimal results. It is therefore crucial to acknowledge and address these challenges meaningfully.

Currently, mammalian healing of wounds are segregated into three distinct phases: inflammation, new tissue formation, and remodeling (Reinke and Sorg, 2012; Škovranová et al., 2022). Inflammation is presented as the first phase in this process. Inflamed sites are first populated by leukocytes during the inflammatory phase (Diegelmann and Evans, 2004). In addition to removing bacteria and debris, they release factors that initiate wound healing. The phase ranking second in mammalian wound healing is tissue formation, during which new (connective) tissue is generated to replace damaged or lost tissue. The proliferation and migration of many cell types, such as fibroblasts, endothelial cells, and keratinocytes, occur during the tissue development phase. These cells work together to produce collagen and other extracellular matrix (ECM) components that provide structural support to the healing tissue. The final phase of mammalian wound healing is the remodeling phase. During this phase, active repairing tissue changes to ensure proper function and structural integrity. These modifications include the cessation of active healing, cell decrease via relocation or death, and wound closure by myofibroblasts to seal wounds and form fibrous scar tissue composed of disordered ECM deposits. (Cesarz and Tamama, 2016).

Regeneration vs Scarring

Regeneration

Tissue repair and regeneration are complex processes involving various cellular and molecular mechanisms (Reddy et al., 2019). Whole-body regeneration (WBR) is a fascinating phenomenon observed in various lower animals. It refers to the ability of certain animals to regenerate any missing tissue, including the entire body (Knapp and Tanaka, 2012; Qarri and Rinkevich, 2023; Srivastava et al., 2014). This remarkable capability has been studied in different model organisms, shedding light on the mechanisms underlying regeneration. For example, echinoderms, such as sea urchins and sea stars, have been used as model organisms to study tissue and whole-body regeneration (Wolff and Hinman, 2021). These animals have provided valuable knowledge about regenerative mechanisms at various life stages. Recent research has focused on investigating regeneration in echinoderm larvae, which can serve as a new system for understanding regenerative processes in basal deuterostomes (Wolff and Hinman, 2021). Studies on *Nematostella vectensis*, a sea anemone, have uncovered the need for neuronal subtypes during regeneration, degrowth, and growth (Havrilak et al., 2021).

Mammals and humans, on the other hand, have limited regenerative capabilities compared to simpler organisms (Massoz et al., 2021). Certain organs and tissues in mammals exhibit regenerative capacity. For example, non-mammalian vertebrates such as zebrafish, can effectively regenerate damaged central nervous system (CNS) tissue through the mobilization of neural stem cells (NSCs) and progenitors. Conversely, adult mammals such as mice and humans have a restricted regenerative capacity in the CNS (Shimazaki, 2016). Repair can restore the primary action of injured tissue in cases where morphological regeneration is absent. For instance, after partial liver hepatectomy or lobectomy, the leftover liver organ expands to make up for the missing tissues without reestablishing the original morphology. Interestingly, some mammals have shown remarkable regenerative capacities in certain tissues. For example, African spiny mice (Acomys) have been found to exhibit complete regeneration of sebaceous glands, dermis, hair follicles and cartilage following injury, in a scar-less manner. This proposes that well-evolved creatures might hold a latent ability to regenerate than normally perceived (Ito et al., 2007; Seifert et al., 2012).

Scarring

The intricate processes of chronic wound healing and scarring encompass a range of cellular and molecular events. The skin acts as a protective barrier, and compromise to this barrier can result in chronic wounds and scars (Panayi et al., 2020, Potter et al., 2019; Sullivan and Myers, 2022). In some cases, the wound-healing process is deranged, leading to the formation of hypertrophic or keloid scars (M. G. Visha and Karunagaran, 2019). Pathological scarring is characterized by excessive proliferation and differentiation of fibroblasts into contractile myofibroblasts which excessively deposit extracellular matrix, rendering the repaired tissue as non-functional. In normal wound healing, the repair process leads to the formation of scar tissue, which is a fibrotic response that occurs in adult skin. However, scar formation can be undesirable and lead to functional and aesthetic complications (Chadwick et al., 2012). The effects and impact of scarring in the wound-healing process are significant in terms of tissue function and biomechanical strength (Brockes et al., 2004).

Conversely, it is interesting to note that primitive mammalian embryos heal wounds without scars, disclosing latent regenerative abilities. One approach to scar prevention and regenerative healing is to study scarless healing in fetal mammals. Fetal skin wounds have been shown to undergo regeneration without scar formation, which correlates with reduced inflammation compared to scarring in adults (Seifert et al., 2012). Overall, while scarring plays a role in restoring homeostasis after injury; it also highlights differences between embryonic vs adult responses during the wound healing process whereby embryonic cells exhibit less-differentiated inflammatory behavior than differentiated adult cells. Growth factors and ECM remodeling are also involved in the healing of wounds and scar generation. Transforming growth factor-beta (TGF-β) is a key regulator of ECM synthesis and deposition, and its dysregulation can contribute to excessive scar formation (Boateng et al., 2008). Targeting the TGF-β signaling pathway may be a potential therapeutic approach for scar prevention (Liu et al., 2006). Other growth factors, for example, epidermal development factor (EGF) and acidic fibroblast development factor (aFGF) have also been studied for their potential to promote wound healing and reduce scars post-injury (Xu et al., 2018).

Skin Introduction

Skin is the largest organ in the human body and assumes a fundamental part in safeguarding internal tissues and organs from environmental hazards/assaults (Liu et al., 2022). The design of the skin comprises three principal layers: the epidermis, dermis, and subcutaneous tissue (Hodge et al., 2022; Xiang et al., 2022). The outermost layer of the skin is constituted by multiple layers of epithelial cells, collectively known as the epidermis. These cells are constantly being renewed and sloughed off, ensuring the maintenance of a healthy barrier (Simon and Abdelmalek, 2012; Wu et al., 2021). The composition of this structure comprises multiple sublayers, among which are the stratum corneum (composed predominantly of deceased skin cells), stratum granulosum, stratum spinosum, and stratum basale (where new skin cells are formed). The epidermis protects against UV radiation, pathogens, and dehydration (Busco et al., 2020). The dermis, situated beneath the epidermis, constitutes a denser stratum consisting of connective tissue, blood vessels, hair follicles, and sweat glands. It serves the purpose of offering structural reinforcement to the skin and contains collagen and elastin fibers that give skin strength and elasticity (Farage et al., 2013). The subcutaneous tissue, also known as the hypodermis, lies beneath the dermis and is primarily composed of fat cells that provide insulation and serve as an energy reserve (Kao et al., 2019). Skin also prevents the entry of harmful microorganisms, allergens, and environmental pollutants (Elias and Choi, 2005). The sweat glands present in the skin aid in maintaining body temperature by secreting sweat, which facilitates the cooling of the body through evaporation. Blood vessels in the skin can dilate or constrict to regulate blood flow and heat exchange (Holick, 2007). The skin contains numerous sensory receptors that detect touch, pressure, temperature, and pain. These receptors allow us to interact with our environment and respond to stimuli (Oliveira et al., 2023).

Mouse skin exhibits some key differences in structure compared to human skin, particularly in the context of fibroblasts and wound healing (Kim et al., 2023). While the basic three-layer structure of the skin is present in both humans and mice, mouse skin has a thinner and flatter epidermis and a less pronounced dermis compared to human skin (Niu et al., 2022). Additionally, mouse skin has a higher density of hair follicles and a deeper muscular layer than human skin (Wang et al., 2015). The differences in skin structure between mice and humans have important implications for wound healing (Yu et al., 2022). In mice, full-thickness wounds primarily heal through contraction, which is the process of the wound edges coming

closer together due to the contraction of underlying connective tissues (Kim et al., 2023). In contrast, humans primarily heal small wounds through the proliferation of surrounding cells (Muhammad et al., 2013). In mouse skin, fibroblasts play a significant role in wound healing but with notable differences compared to human skin. In mouse skin, fibroblasts are present in higher numbers due to the higher density of hair follicles. While mice primarily heal through wound contraction humans rely on re-epithelialization and granular tissue formation for wound healing, so it is difficult to model the healing patterns of humans in mice (Iimura et al., 2016; Meyers et al., 2019; Yang and Su, 2010). To address this limitation, Galiano et al. (2004) developed the splinted full-thickness model in mice whereby researchers were able to achieve a more "human-like" pattern of wound healing by applying occlusive coverings to wounds (Luparello et al., 2020). In human skin, fibroblasts are found primarily in the dermis and are responsible for collagen production and wound contraction. They play a critical role in wound healing by producing collagen and other ECM components. These fibroblasts migrate into the wound bed and create a supportive scaffold for the migration of keratinocytes, the predominant cell type in the epidermis. This coordinated migration of fibroblasts and keratinocytes is essential for re-epithelialization (Mapoung et al., 2021; Sagástegui-Guarniz et al., 2021). Understanding the differences between human and mouse skin is crucial to developing effective treatments for chronic wounds.

Fibroblasts

Fibroblasts are versatile cells with diverse embryological origins. differentiation pathways, and functions. These spindle-shaped cells typically arise from various tissue sources, including bone marrow-derived mesenchymal stem cells, local tissue-resident fibroblasts, and even epithelial-to-mesenchymal transition (EMT) of neighboring epithelial cells. The diverse origins of fibroblasts disclose a heterogeneity of this class of cells (Driskell et al., 2013; Gurtner et al., 2008; Hinz, 2007). One key aspect to consider is the role of fibroblasts in the healing process. Fibroblasts are a type of connective tissue cell that plays a crucial role in wound healing by producing collagen, a protein necessary for the formation of new connective tissue, which is restructured in wound healing (Meiners et al., 2018; Muhammad et al., 2013; Sivaraj et al., 2021).

In skin, different subtypes of fibroblasts, such as dermal, reticular, and papillary fibroblasts, have distinct functions and contribute to the different phases of skin development and wound

healing. The strongest contribution for human skin wound healing is made possible by dermal fibroblasts, while papillary fibroblasts promote healing without scarring and have the potential to stimulate the earlier phases of hair follicle growth (Dermal fibroblasts 2017). Dermal fibroblasts are not passive cells but actively participate in wound healing by secreting signaling molecules that regulate inflammation, cell proliferation, and communication with other cells involved in the healing process (Stunova and Vistejnova, 2018).

Reticular and papillary fibroblasts have different gene expression patterns, ECM deposition, and angiogenic potential (Haydont et al., 2020; Mauroux et al., 2020). They contribute to the formation of distinct capillary networks and regulate angiogenesis through secreted and ECM-bound factors (Hogervorst et al., 2018). Reticular fibroblasts are primarily responsible for producing and maintaining the reticular fibers, which are a type of collagen (Type III collagen) (Haro and Orsulic, 2018; Textor et al., 2016). In the context of wound repair, these fibroblasts play a crucial role. They are the ones responsible for initiating the healing process by emigrating toward the wounded location and generating a dermis comprised of collagen that is enriched (Oh et al., 2022). The presence of reticular fibroblasts is thought to be essential for the formation of a strong and supportive dermal layer, which is necessary for proper wound healing and tissue regeneration.

On the other hand, papillary fibroblasts encompass the later stages of wound healing where they enter the wound site at a later stage and are responsible for the re-epithelialization of the open wound (Krieg et al., 2007; Ojeh et al., 2015). Reformation of the epidermis and the generation of hair follicles are important stages for restoring the normal appearance and function of skin after injury (Hu et al., 2018; Leng et al., 2020). Fibroblasts located at the dermo-hypodermal junction have wider latency for differentiation and display specific gene expression profiles related to ECM synthesis and tissue organization (Wu et al., 2022). Fibroblasts are also involved in tissue repair and fibrosis, and their heterogeneity and distinct functional roles have been identified across various organs (Talbott et al., 2022). Each fibroblast subset performs unique responsibilities that are crucial to promoting and regulating specific phases of wound healing. Overall, fibroblasts exhibit a kaleidoscope of cell types and collectively are critical in supporting all wound healing phases (Saraswati et al., 2019).

Specialized fibroblasts in Wound Healing

Nowadays, fibroblasts are seen as active participants in many immunological processes rather than simply providing structural support (Jordana et al., 1994). Wound healing necessitates a precise spatiotemporal coordination of three successive phases during which certain mesenchymal cell types, known as proinflammatory fibroblasts and myofibroblasts, emerge and disappear in response to injury. Initially, leukocytes enter the wound bed during the early inflammation phase to assist with anti-microbial and cellular debridement that creates a temporary milieu that is hypothesized to aid the following stages of wound healing (Correa-Gallegos et al., 2021; Correa-Gallegos and Rinkevich, 2022; Eming et al., 2014).

Proinflammatory fibroblasts

Proinflammatory fibroblasts are a specialized subset of fibroblasts that appear during the inflammatory phase and play a crucial role in promoting and sustaining chronic inflammation in various diseases such as fibrosis, rheumatoid arthritis, and cancer (Li et al., 2014). Furthermore, these fibroblasts attune to proinflammatory cues, such as IL-1β, TNF, reactive oxygen species, and TGF β, which further amplifies their proinflammatory phenotype and promotes the progression of chronic inflammation (Li et al., 2014; Potluri et al., 2022; Takeuchi and Gotoh, 2023). Pro-inflammatory fibroblasts are attracted to the site of injury and secrete factors that promote angiogenesis and differentiate into myofibroblasts, the next phase of wound healing, where mature scars are formed (Xiao et al., 2017). These fibroblasts also secrete pro-inflammatory cytokines that stimulate the inflammatory response and promote cell migration during wound remodeling, without which wound healing is altered (Asparuhova et al., 2019). For example, fibroblasts in diabetic wounds exhibit altered plasticity and function, highlighting the importance of understanding the molecular mechanisms that regulate their behavior in wound healing (Shao et al., 2020).

Furthermore, the activity of fibroblasts is influenced by numerous factors. For example, the low molecular weight factor Pro-Hyp initiates fibroblast growth. Extensive research has unveiled the crucial role of this factor in expediting wound healing and unlocking its powerful therapeutic capabilities for chronic wounds (Sato et al., 2020). Research has demonstrated the utilization of ozone oil that stimulates the healing process of wounds by boosting the movement of fibroblasts through the PI3K/Akt/mTOR signaling pathway. (Xiao et al., 2017). Vitamin C

has pleiotropic effects on wound healing and can modulate the function of fibroblasts in the wound microenvironment (Mohammed et al., 2016). Additionally, fibroblasts produce cytokines of proinflammatory state in the presence of hyaluronic acid, promoting the inflammatory response and stimulating hyaluronan synthesis by endothelial cells (Asparuhova et al., 2019). Overall, pro-inflammatory fibroblasts play an early and significant role in wound healing and tissue repair, and their dysfunction can lead to delayed healing and tissue damage in various diseases such as chronic open wounds, venous insufficiency, aging, and diabetes.

Myofibroblasts

Myofibroblasts are classified by their contractile properties and expression of α-smooth muscle actin (α-SMA), and play diverse roles in pathological processes (Masur et al., 1996). Upon tissue damage, myofibroblasts are directed to the location of damage and are responsible for wound closure through the synthesis and contraction of the extracellular matrix (ECM) (Kollmannsberger et al., 2018). While myofibroblasts contribute to wound contraction during the healing process, their prolonged presence in tissues is a key driver of fibrosis and/or contractures (Tai et al., 2021: Maquart et al., 1988). By generating traction and contractile forces, both proinflammatory and myo-fibroblasts contribute to wound healing (Li & Wang, 2011). Myofibroblasts differentiate from fibroblasts during wound healing, but their exact tissue and embryonic origins are incompletely understood (Masur et al., 1996). For example, myocardin-related transcription factor (MRTF)-A (Velasquez et al., 2013) and muscleblind-like1 (MBNL1), participate actively in the transformation of fibroblasts into myofibroblasts (Davis et al., 2015). Urokinase receptor cleavage is also a crucial step (Bernstein et al., 2007) akin to TGF-ß1 activation which promotes the differentiation of fibroblasts into contractile myofibroblast state (Tai et al., 2021).

Adult connective tissues, normally have low numbers of these fibroblast populations. However, the presence of wound healing-related cytokines amplifies their cell numbers and induces their differentiation. During the proliferative phase of wound healing, the number of myofibroblasts drastically increases. These cells are involved in tissue remodeling and collagen synthesis (Smith, 2018). Myofibroblasts further participate in the remodeling of the wound through phagocytosis and the expression of transglutaminase and matrix metalloproteinases. As wound healing progresses, the ECM is contracted by its resident myofibroblasts to re-appose adjacent

wound margins, and myofibroblasts eventually disappear or deactivate through apoptosis and/or senescence as wounds close and heal (Myrna et al., 2009).

In conclusion, the involvement of myofibroblasts in wound healing is a critical and complex process. These specialized cells provide contractile forces and generate ECM, facilitating wound closure (Grounds et al., 2005). Their recruitment and differentiation from fibroblasts are triggered by various signaling pathways and factors released during the inflammatory phase of wound healing (Gushiken et al., 2017; Rouabhia et al., 2013; Sim et al., 2022, p. 2022). Additionally, myofibroblasts secrete cytokines and growth factors that contribute to the inflammatory response and recruitment of immune cells, further aiding in tissue repair. While myofibroblasts are absent in healthy skin, their presence and activation in response to tissue damage are essential for effective wound healing. Understanding the biology and heterogeneity of these cells is essential for developing targeted therapies for chronic wounds and pathological conditions characterized by fibrosis.

Migration dynamics

Fibroblasts differentiate post-injury through molecular cues that dictate their transition into specialized fibroblast subtypes. This differentiation cascade is spatiotemporally regulated by definite checkpoints. A previous study from our lab identified Engrailed-1 (En1) transcription factor-positive fibroblasts during embryonic development (termed EPFs) to be the driving force that contributes to scarring post-injury (Jiang et al., 2018). EPFs accomplish this by swarming towards the center of the wound and replacing the original connective tissue with a dense ‘plug’ of fascia-born matrix protein fibers and macromolecules (Correa-gallegos et al., 2019; Huang et al., 1978; Palmieri et al., 2003). Understating the molecular dynamics by which this is achieved is thus both important and challenging. Consequently, in one of my previous publications (Ramesh et al., 2022) we developed a novel experimental setup that emulates EPF dynamics throughout the process of scar formation and wound closure. Earlier experimental designs that aimed to unravel fibroblast differentiation in wounds caveated primarily by a non-native environment that failed to comply with the original composition of the dermis (Abd et al., 2016; Li et al., 2020). Previously, the functions and involvement of fascia in wound healing were limited because of a lack of tools and models to explore the behaviors of cells in their native fascia environment. To answer all these avenues, our ex-vivo model termed “scar-like tissue in a dish” (SCAD) was designed. In this SCAD model, 2mm full-thickness biopsy

punches are made of post-natal day 0/1 (P0/P1) mice or the back skin of adult mice. SCADs were then cultured in media and for up to 5 days together with modulators to explore the potential role of fibroblasts in healing wounds. We further used this model in another work published in our lab (Jiang et al., 2020) where the model was utilized to identify the role of N-cadherin in the swarming of EPFs in the wound bed. It was noted that intercellular adhesion is important for the fibroblasts to be able to initiate skin contraction and scar formation. Inhibition of N-cadherin prevented the aggregation of the EPFs, thus suggesting that it plays a significant role in minimizing scars and can be a suitable candidate for therapeutic studies.

A map of fibroblast states in wound healing

Recent studies with single-cell transcriptomics on skin (Foster et al., 2021; Joost et al., 2020) and internal organs (Adams et al., 2020; Kuppe et al., 2021) have brought new insights into fibroblast cell heterogeneity. However, the exact cellular and molecular workflow that is involved in the process of wound healing remains unknown. Studies have shown that fibroblasts react differently when isolated from different regions of the body and different wound areas (Abbasi et al., 2020; Shook et al., 2018). Moreover, fibroblast progenitor characteristics, origins, and differentiation trajectories during wound healing are not well understood. Thus, understanding and regulating wound healing stages requires a thorough understanding of these events.

Fibroblast subtypes in skin are defined by their location and named accordingly. For example, the papillary dermis is composed of papillary fibroblasts, below them in the reticular dermal region lie the reticular fibroblast fraction and in the deepest connective tissue layer of the skin, hypodermis, lies a connective tissue layer called fascia that comprises of fascia fibroblasts (Correa-Gallegos et al., 2019). As already stated before, a previous study from our lab showed that myofibroblasts originate from EPFs (Jiang et al., 2020; Rinkevich et al., 2015). However, these EPFs are found in every connective tissue layer of the skin, and it is difficult to pinpoint the exact anatomic location where progenitors reside or their exact differentiated paths into myofibroblast that upholds wound healing. Previous studies showed that both fascia and reticular fibroblasts take part in generating skin scars (Driskell et al., 2013; Rinkevich et al., 2015) and a more recent study from our group has revealed that fascia fibroblasts have a higher scar-forming capacity than dermal fibroblasts (Correa-Gallegos et al., 2019). Therefore, in the need to illuminate the exact route of how any fibroblast type arises in wound healing, in our

recent publication (Correa-Gallegos, Ye, Dasgupta, et al., 2023) we discovered $CD201^+$ progenitors in the fascia, promote skin wound healing by generating specialized cell types in a spatiotemporal sequence. We identified a new fibroblast cluster that dictates spatiotemporal topographies of wound healing as they differentiate sequentially into specific fibroblastic cell types. In addition to the already-known reports that myofibroblasts are prevalently found in the upper regions of the wound (McGrath and Hundahl, 1982) we identified key differences in the fibroblast activity in the different layers of the skin. $CD201^+$ fibroblast progenitors are normally located within the very deep layers of skin, and they follow a spatial bottom-to-up command in response to an injury. The intricate niches of coming to this conclusion are detailed below through a variety of *in silico, in vivo* and *ex vivo* studies.

Results

Skin wounds contain diverse fibroblasts

scRNAseq and genetic lineage tracing of excisional fibroblasts were used to investigate the biological transition of fibroblasts during wound healing. The $En1^{Cre}$ x $R26^{mTmG}$ line was utilized to permanently label EPFs with membrane-bound GFP. Bilateral, full-thickness excisional wounds in mice were followed by FACS-sorting the mesenchymal-enrichment fraction, which included both GFP^{+} and GFP^{-} fibroblasts. Total mesenchymal cells were sequenced in an unbiased manner at relevant days post-injury to include all the important phases of wound healing such as inflammation, proliferation, and remodelling. Seven unique fibroblast clusters were identified in the initial stages (figure 1a); clusters 0–2 were observed in both wounded and intact skin, whereas clusters 3-6 were predominant in tissues that had been wounded. The expression of a collection of markers already available for local myofibroblasts, reticular, fascia, and papillary fibroblasts was used to identify the clusters as well. The papillary profile scored best in Cluster 0, which was followed by the fascia profile in Cluster 1 and the reticular profile in Cluster 2. The characterization of the clusters was performed by Donovan and is explained in more detail in the article recently published by us (Correa-Gallegos, Ye, Dasgupta, et al. Nature 2023). Additionally, we discovered a particular fibroblast marker of the fascia cluster with CD201 (Procr), a marker of progenitor mesenchymal cells in the spleen and muscle (Tan and Watanabe, 2017; Uezumi et al., 2016).

As the next steps, we wanted to identify the origin of myofibroblasts and used an algorithm named Partition-based graph abstraction (PAGA) to calculate through bioinformatic interpretations how these clusters are interconnected (figure 1b). The preliminary investigation disclosed an intricate network of connections between all fibroblast subtypes and followed similar findings from other studies. For example, our analysis revealed the lack of a prominent role of papillary fibroblasts in wound healing (Driskell et al., 2013) and a major role played by the reticular and fascia fibroblast fractions. Our findings also indicated that myofibroblasts originate from proto-myofibroblasts and they arise in turn from pro-inflammatory subclusters which are derived from fascia fibroblasts (figure 1b).

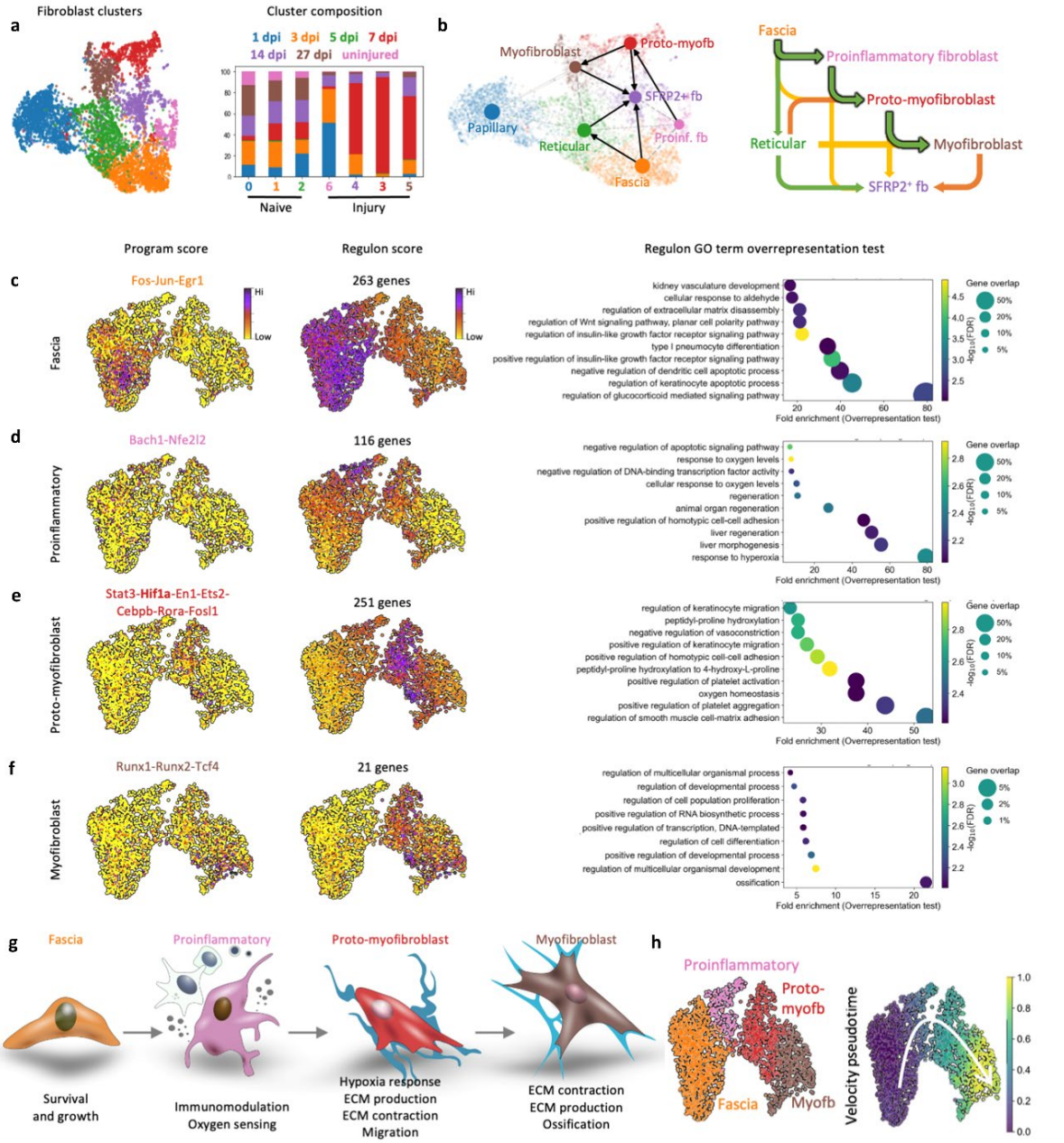

Figure 1 | RNA sequencing of stromal cells during wound healing reveals specialized states, a stepwise differentiation linked to wound healing phases. a. Stromal cell clusters represented in Uniform manifold approximation and projection (UMAPs) (left) and their mode of organization in uninjured and injured conditions (right). **b.** Left, PAGA-associated links overlayed on fibroblast UMAPs. proinf., proinflammatory. Right, fascia-to-myofibroblast differentiation graphic scheme as predicted. **c-f.** UMAPs of program score (left) and regulon score (center) and GO term overrepresentation (right) for the fascia (c), proinflammatory (d), proto-myofibroblast (e), and myofibroblast states (f). **g.** Diagrammatic representation of each fibroblast subtype according to their roles derived from *in silico* tests. **h.** Recalibrated representation of fascia-to-myofibroblast differentiation state marked by colors (top) and scored according to velocity pseudotime. Illustrations were made by Donovan and modified from Correa-Gallegos, Ye, Dasgupta, et al., Nature 2023 under Creative Commons Attribution 4.0 International License.

Our analysis of the genetic programs of each fibroblast cluster revealed that they have distinct functions. Fascia fibroblasts promote cell survival and growth, while proinflammatory fibroblasts direct immunomodulation and oxygen sensing (figure 1c-d). Proto-myofibroblasts control migration, adhesion, and collagen production which reveal a shift from

immunomodulatory activities to matrix-producing roles, underscoring the transition that occurs in wound healing phases from inflammatory to proliferation and remodelling. Finally, myofibroblasts influence the terminal differentiation of the fibroblasts (figure 1e-f). These newly discovered differentiation paths and phenotypes suggest that fascia fibroblasts morph into proinflammatory, proto-, and myofibroblasts and suggest that they have a crucial role in the successful progression of wound healing phases (figure 1g).

Therefore, we recalibrated the initial clustering based on our findings and previous literature to the trajectory where the transition of fascia fibroblasts to the myofibroblast state is a sequential process through the intermediate proinflammatory and proto-myofibroblast stages and used it for the next experiments (figure 1h). The 'regulon' analysis and the interpretation-based recalibration of UMAP analysis were also performed by Donovan and are explained in more detail in our paper (Correa-Gallegos, Ye, Dasgupta, et al. Nature, 2023).

Differentiation capacity of CD201^{+} cells

We wanted to validate the differentiation stages identified *in silico* in relation to wound healing stages *in vivo*. First and foremost, we affirmed the articulation profiles of group explicit markers in mouse skin wounds at 3- and 7-days post-infection, revealing PDPN^{+} proinflammatory, pSTAT3^{+} proto-myo and RUNX2^{+} myofibroblast peaking at 3 and 7 days respectively (figure 2a) (the data analysis was supported by Donovan). Then, we investigated the occurrence of these markers in wounds. At 3dpi (days post-injury), we observed the PDPN^{+} fibroblasts to be restricted to the deeper regions of the wound while at 7dpi, the RUNX2^{+} fibroblasts were limited to the upper wound regions only. The pSTAT3^{+} fibroblasts had no distinct spatial restrictions and were present throughout the entire wound area (figure 2 b-d) (staining and imaging was performed by Donovan). This observation led us to believe that some specific signals were guiding the fibroblast differentiation in a deep wound to superficial wound orientation (figure 2e).

Next, we wanted to address our hypothesis that myofibroblasts originate from CD201^{+} fascia fibroblasts. To do this, we crossed CD201^{CreER} lineage mice with R26^{Ai14}, which reports stable fluorescence, to enable us with a persistent expression of TdTomato in CD201-expressing cells of the progeny following tamoxifen administration (figure 2f). In normal skin, we identified

labelled fibroblasts primarily present in the fascia compartment, while endothelial, epithelial, and immune cells were minimally marked.

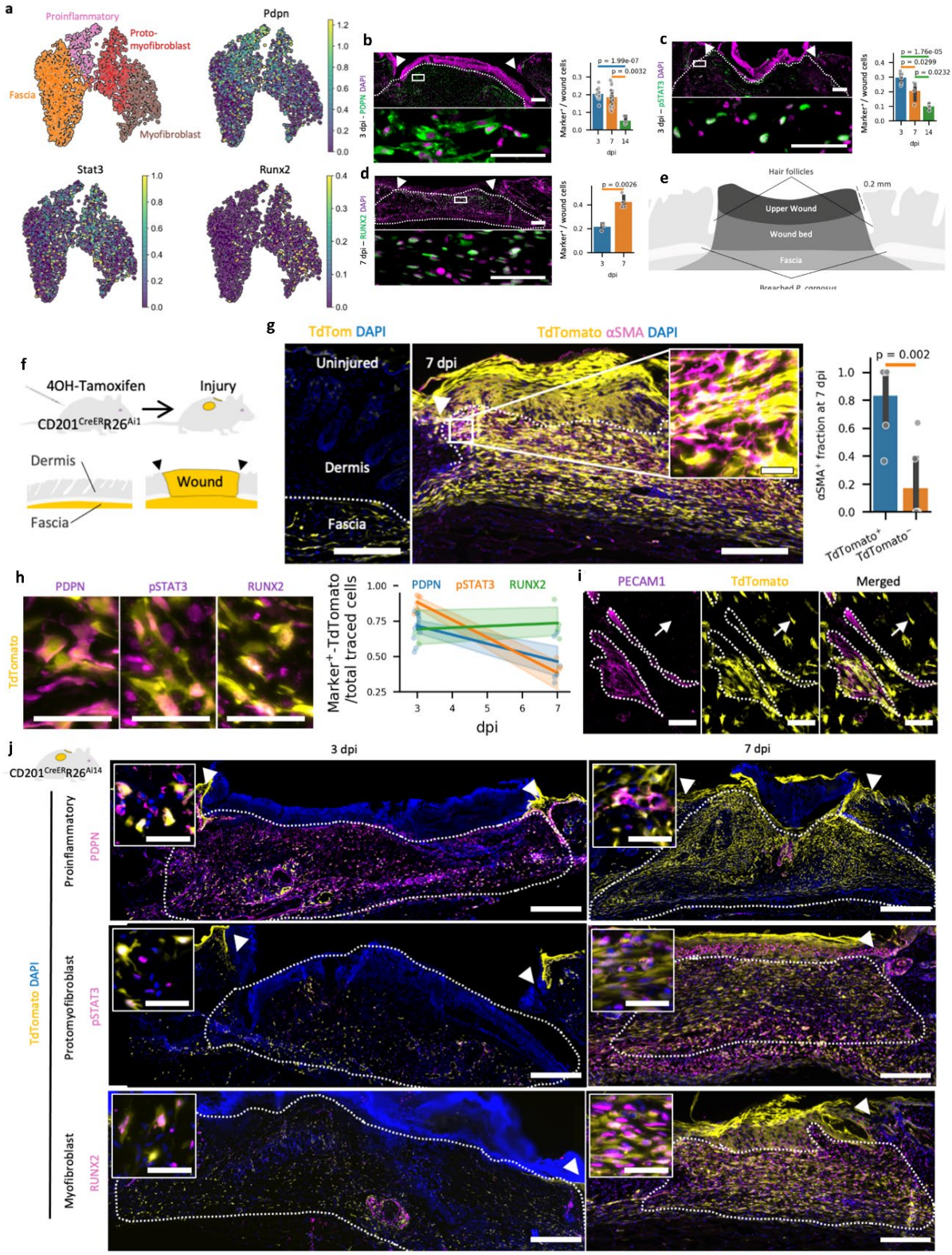

Figure 2 | CD201^{+} fascia fibroblasts undergo specialized differentiation during wound progression, exhibiting spatial and temporal patterns during this transition. a. Representation of fascia-to-myofibroblast differentiation state marked by colors (top left) and each relevant cell state marker (top right and bottom panel). **b-d.** Immunostaining (left) and analyzing marker-expressing cell quantifications (right) at various time points after injury in wounds of 3- or 7-dpi for PDPN (b), pSTAT3 (c), and RUNX2 (d). Staining for PDPN contained imaging of n = 16 (3 dpi), 12 (7 dpi), and 3 (14 dpi) samples.

pSTAT3 staining contained 6 (3 dpi) and 4 (7 and 14 dpi) images of sections and 3 (3 dpi) and RUNX2 had 4 (7 dpi) images. 3 biological repeats for every time point were collected and investigated. Rectangular inserts inside lower magnification images (top) are represented in the bottom panel in high magnification. The wound area is marked by dotted lines with arrows to depict the original injury location. **e.** Graphics depicting the wound areas studied, as well as the spatial clues that mark them. **f.** Graphic illustration showing methodology to follow $CD201^+$ fascia fibroblast differentiation course in a progression of healing wounds. **g.** Representative histology of normal (left) 7 dpi wound of $Cd201^{creER}$ x $R26^{Ai14}$ and (middle) stained for αSMA. Right, for 6 wounds from 3 animals, the involvement of $CD201^+$ fibroblasts to the myofibroblast reserve was assessed using two-tailed Student's t-tests. The wound area is marked by a dotted line. Arrows depict the original injury location. The rectangular drawn area illustrates a magnified outlook. **h.** High-resolution characteristic images to depict the expression of PDPN, pSTAT3, or RUNX2 in the lineage labelled cells(left) measured at 3 and 7 dpi (right). A minimum of 3 animals were used to obtain the results. **i.** PECAM1, an endothelial marker, stained in the healthy fascia of $Cd201^{creER}$x $R26^{Ai14}$mice detected lineage labelled cells far from vascular regions. **j.** Expression of PDPN (top), pSTAT3 (middle), and RUNX2 (bottom) in TdTomato-marked fascia-traced cells on 3 (left) and 7 dpi (right) wounds as depicted in lower and higher magnification (expanded). Rectangular inserts inside lower magnification images are represented in the bottom panel in high magnification. Scale bars: 500 μm (i and g, j low mag images) and 50 μm (g and h, j expanded views). Only figure panels b, c, d, i and illustrations a, e, f have been made by Donovan and modified from Correa-Gallegos, Ye, Dasgupta et al., Nature 2023 under Creative Commons Attribution 4.0 International License.

Likewise, in 7-dpi wounds, the majority of $TdTomato^+$ cells were fibroblasts, distinguishing them from endothelial, epithelial, or immune cells. Additionally, it is noteworthy that of all the αSMA^+ myofibroblasts, the $TdTomato^+$ cells accounted for 83% of cells and were derived from $CD201^+$ progenitors (figure 2g) (the *in vivo* work with the animals and tamoxifen induction was supported by Donovan and all remaining post-processing and analysis were performed by me).

Then, we asked if $CD201^+$ fascia fibroblasts diverged into the subsequent populations identified *in silico* upon injury *in vivo* in mice. Upon transition from inflammatory/granulation to granulation/maturation phases, $CD201^+$ markers steadily decreased in the expression levels of proinflammatory and proto-myofibroblast markers, specifically PDPN and pSTAT3, which went down from 71.5% to 46.4% and 88.2% to 38.4% respectively, between 3 to 7 dpi (figure 2h). Alternatively, at 7 dpi, the $CD201^+$ fibroblast lineage expressed the myofibroblast marker RUNX2 by 73.5 percent (figure 2j). The change in marker articulation of $CD201^+$ fibroblasts reveals that their alteration to proinflammatory and myofibroblast states coincides with the progression of wound healing phases. It was further noted that within the uninjured fascia, $TdTomato^+$ fibroblasts exhibited a broader distribution throughout the connective tissue, rather than being confined solely to the perivascular space (figure 2i) (PECAM staining and imaging performed by Donovan).

We then developed a complementary system utilizing the proinflammatory marker PDPN ($PDPN^{CreER}$) under expression of Cre-ER recombinase and generated a system that allowed us to investigate the transition of $CD201^+$ fibroblasts into myofibroblasts, specifically focusing on the intermediate proinflammatory state (figure 3a). To trace the lineage of $PDPN^+$

proinflammatory cells and confirm transition from the proinflammatory state to myofibroblasts, we crossed the PDPN^{CreER} mice with the R26^{mTmG} reporter mouse line. In uninjured skin, GFP^{+} cells were not detected in any healthy un-injured skin compartment of the PDPN^{CreER} x R26^{mTmG} mice.

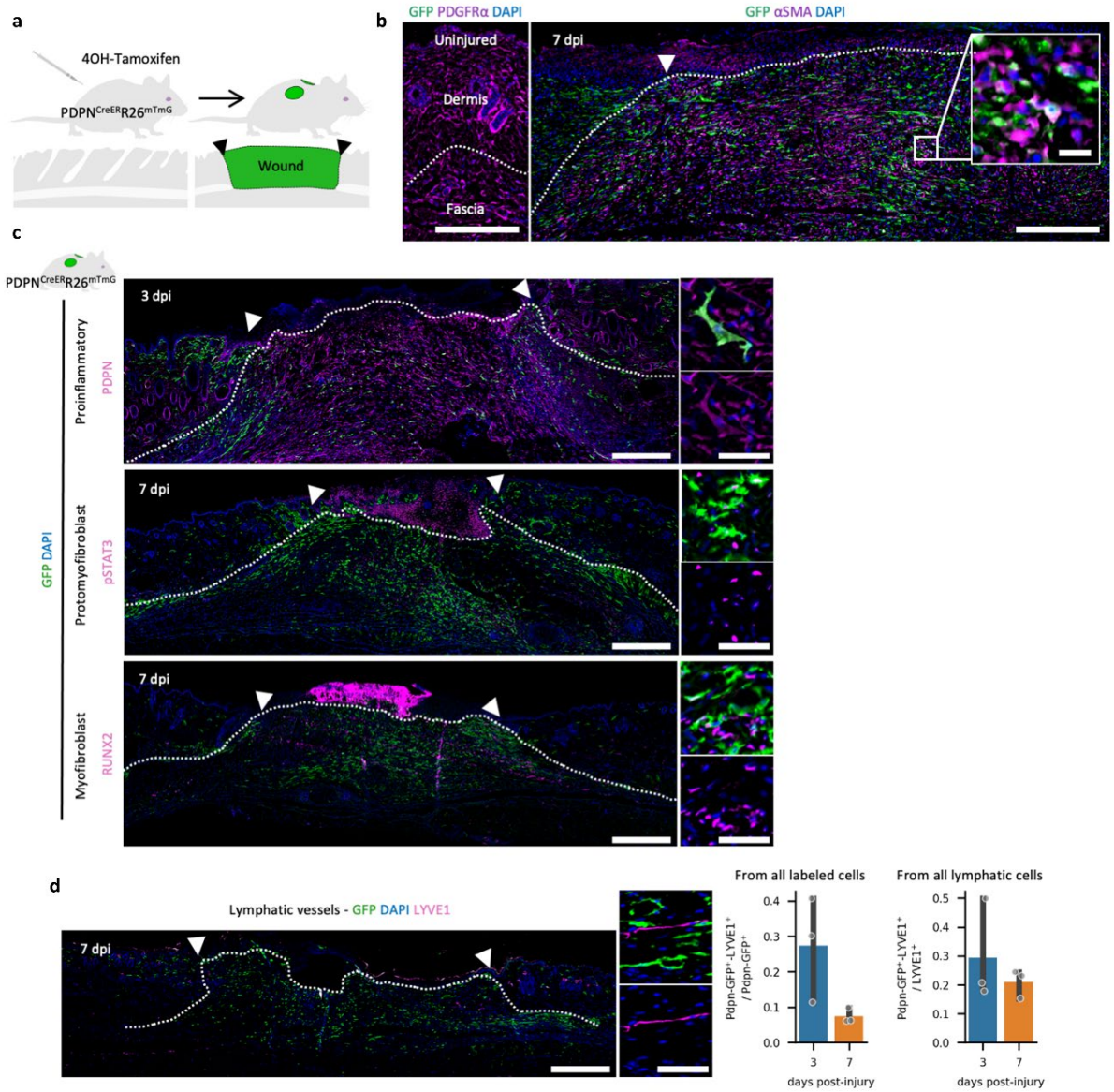

Figure 3 | The manifestation of fibroblast markers in and PDPN^{CreER} x R26^{mTmG} double transgenic line. a. Schematic showing lineage tracing method to follow PDPN^{+} fibroblast differentiation in progression of healing wounds. **b.** Representative images of uninjured skin stained for PDGFRα (left) and a 7-dpi wound (right) of PDPN^{creER}R26^{mTmG} stained with αSMA. The wound area is marked by dotted lines with arrows to depict the original injury location. Rectangular inserts inside lower magnification images are represented in the bottom panel in high magnification. **c.** Expression of PDPN (top), pSTAT3 (middle), and RUNX2 (bottom) in GFP-marked proinflammatory traced cells on 3 and 7dpi shown in lower (left) and higher (right) magnification. The wound area is marked by dotted lines with arrows to depict the original injury location. **d.** Images of LYVE1^{+} lymphatic vessels in injury area at specified time points co-labelled with GFP in both low (left) and high (high) magnifications. Quantification at specified time points of labelled-lymphatic endothelial cells from total lineage labelled and from whole lymphatic vessels in wounds. n = 3 biological repeats. The wound area is marked by dotted lines with arrows to depict the original injury location. Scale bars: 500 microns in low magnification, and 50 microns in expanded view. Only the illustration has been made by Donovan and modified from Correa-Gallegos, Ye, Dasgupta, et al., Nature 2023 under Creative Commons Attribution 4.0 International License.

However, at 7 dpi, a significant number of αSMA/GFP double-positive myofibroblasts, which were determined to be of proinflammatory origin (GFP^+), were detected in the upper regions of the injury area (figure 3b). Additionally, the co-expression of the markers pSTAT3, PDPN, and RUNX2 in the GFP^+ cells at significant time points following injury suggested a sequential progression of proinflammatory fibroblasts into mature myofibroblasts which confirms our initial hypothesis of myofibroblasts and proinflammatory fibroblasts originating from $CD201^+$ progenitors during wound progression (figure 3c).

To evaluate the contribution of $LYVE1^+$ lymphatics to the GFP^+ cell population, we assessed the overall commitment of $LYVE1^+$ lymphatics to this pool. We found only around 33% of GFP^+ lymphatic cells among a mere quarter of all GFP^+ cells were identified as lymphatic cells (figure 3d). As a result, it can be concluded that the majority of the marked cells were inheritors of the pro-inflammatory subfraction. These findings provide confirmation regarding the transformation of pro-inflammatory fibroblasts into myofibroblasts during the process of healing of wounds in skin. Moreover, it is evident that our transgenic systems, $CD201^{CreER}$ and $PDPN^{CreER}$, are capable of effectively tracing the various stages of this conversion.

From these genetic lineage tracing studies, we discover that the subgroup of $CD201^+$ progenitors embark on a transformative trajectory, shaping the destiny of fibroblasts within the confines of wound healing. These progenitors embark on a remarkable journey of metamorphosis, as they transition into proinflammatory fibroblasts in the deeper wound areas, and subsequently into myofibroblast states in the superficial wound area, sequentially.

Impaired $CD201^+$ progenitor differentiation blocks wound healing

Next, we explored whether the transformation of fascia into myofibroblasts is important for healing wounds. We developed an *ex-vivo* model utilizing mouse back skin fascia (figure 4a), to examine the correlation between tissue contraction and fibroblast differentiation. Throughout a six-day culture duration, the transparent fascia explants progressively contracted in size to 50% of their original area before developing into an opaque sphere resembling scar tissue (figure 4b), similar to in vivo fascia in wounds. This observation supported the hypothesis that fascia differentiation into myofibroblasts is crucial for wound healing and scar formation *ex vivo* and *in vivo*. We also observed that in the *ex vivo* system, the fascia fibroblasts transition into myofibroblasts after sequential passage through the pro inflammatory and proto-

myo states (figure 4c), precisely mimicking the differentiation trajectory in vivo. The transformation of CD201^{+} fascia progenitors into proinflammatory fibroblasts occurred within 3 days of culture, showing a significant 4.6-fold rise in PDPN^{+} cells by day 3.

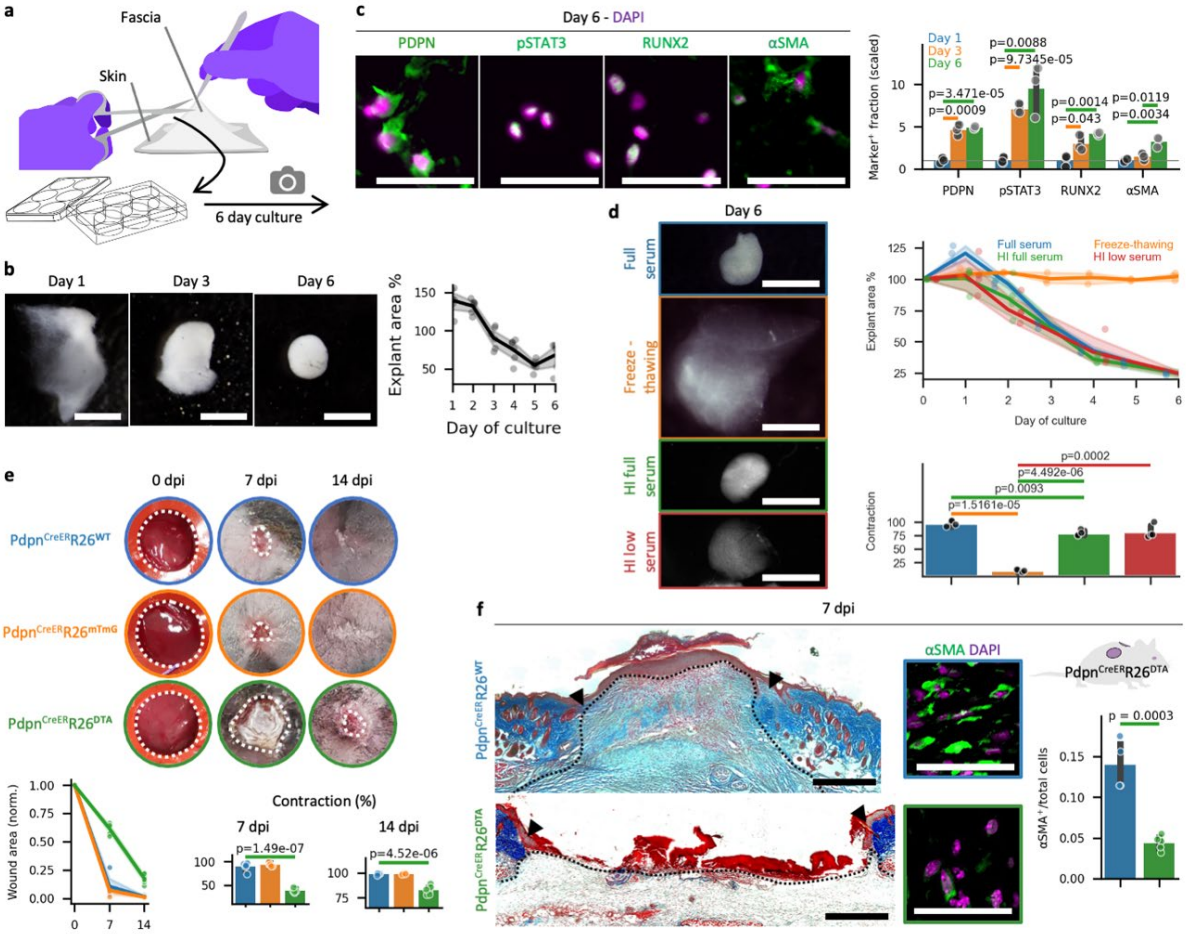

Figure 4 | Impairing the differentiation trajectory impairs the contraction capacity. a. Graphic illustration of *ex vivo* fascia culture. **b**. Photographic visuals of fascia specimens at the relevant culture time points (left) and overall area shrinkage evaluations (right). n = 5 from 3 individual mice. **c**. Tissues stained for PDPN, pSTAT3, RUNX2 or αSMA (left) and corresponding values of positive cell numbers at 1, 3 and 6 days of culture standardized to day 1 values (right). n = 3 biological repeats. **d.** Impact of cell ablation (freeze-thawing) and different serum conditions on fascia explants after 6 days of culture (left) and their subsequent shrinkage area (top right) and total shrinkage (bottom right). n = 3 (freeze-thawing & full serum) and 4 (heat-incapacitated high and minimal serum) biological repeats. HI, heat inactivated. The treatments in the graphs are indicated by the colors of the picture outlines. **e.** Bright-field images of splinted wounds on transgenic lines of PDPN lineage at 0, 7, 14 dpi (top), wound area quantification (bottom left) and contraction percentage at the indicated dpi (bottom right), indicating a delay in healing on removal of proinflammatory fibroblasts. 3 biological repeats generated n = 6 wounds. WT, wild type. **f.** The control (top left) and ablated (bottom left) 7 dpi wounds were subjected to Masson's trichrome staining for analysis. The wound area is marked by dotted lines with arrows to depict the original injury location. High-magnification images of control (top middle) and ablated (bottom middle) 7 dpi wounds stained for αSMA. Right, αSMA^{+} fibroblast cell numbers in wounds. n = 4 (control) and 5 wounds from 3 biological repeats. The treatments in the graphs are indicated by the colors of the picture outlines. Two-tailed t-tests. Scale bars: 2 mm (b, d), 500 µm (f, left) and 50 µm (c and f, middle). Only figure panel d has been created by Haifeng, Disha & Robert, and photos in panel e have been made by Donovan and adopted from Correa-Gallegos, Ye, Dasgupta, et al., Nature 2023 under Creative Commons Attribution 4.0 International License.

However, the emergence of proto-myofibroblasts and myofibroblasts aligned with the contraction of the tissue starting from day 3, resulting in a notable 9.5-fold increase in pSTAT3^{+} cells, a 4.2-fold increase in RUNX2^{+} cells, and a 3.2-fold increase in αSMA^{+} cells by day 6 (figure 4c). It was also noticed that cell ablation exerted an inhibitory influence on explant

contraction. Conversely, when heat-incapacitated or minimal serum medium was utilized, the impact on overall contraction was insignificant which implies that the control of fascia fibroblast differentiation is a cellular driven process (figure 4d). These findings offer supporting evidence for the notion that the transformation of fascia fibroblasts into contractile states plays a crucial role in facilitating tissue contraction. (Only cell ablation, heat-inactivated, low serum experiments were supported by Haifeng, Disha and Robert as indicated in our paper Correa-Gallegos, Ye, Dasgupta et al., Nature 2023. Every other ex vivo experiments and all the data analysis was performed by me). As a next step, we wanted to check the potential of the proinflammatory fibroblasts in the progression of healing wounds. To do this we utilized a cre-controlled recombination system to express diphtheria toxin protein ($R26^{DTA}$) that promotes specific cell ablation in cells expressing the target gene. Therefore, we conducted genetic ablation of $PDPN^{+}$ fibroblasts using a $PDPN^{CreER}$ mice crossed with the $R26^{DTA}$ line. When double transgenic mice were exposed to tamoxifen induction, proinflammatory fibroblasts expressing $PDPN^{+}$ marker underwent cell death prior to transiting into the contractile myofibroblast state. We further used the splinted wound model to negate the effect of other contracting tissues such as muscle and to better represent the human wound healing process. We used both control animals ($PDPN^{CreER}$ x $R26^{WT}$ and $PDPN^{CreER}$ x $R26^{mTmG}$) and treatment groups ($PDPN^{CreER}$ x $R26^{DTA}$) and performed experiments to follow wound closure in all groups. Where the wounds in the control groups showed normal progression of healing amongst 7 and 14dpi, the treatment group with ablated proinflammatory fibroblasts showed poor healing sequence and failed to close even after 14dpi (figure 4e). (the *in vivo* work with the animals and tamoxifen induction were supported by Donovan and all remaining post-processing and analysis were performed by me). Histological studies revealed that 7dpi wounds in the control group had a significantly higher wound bed architecture and matrix composition when matched against the treatment group and there was even very little progression of healing stages within them. Particularly, the αSMA^{+} fraction in the treatment group was reduced by almost 71% compared to the control group (figure 4f).

Based on our comprehensive research findings, it can be inferred that the fibroblasts originating from the fascia significantly contribute to the effective progression of the various phases involved in the wound healing process. The proinflammatory fibroblasts, in particular, were found to derive from fascia progenitors and assume a critical role in ensuring a successful healing. (only the ablation in vivo work and bright field imaging were supported by Haifeng

and can be found in in our paper Correa-Gallegos, Ye, Dasgupta et al., Nature 2023. The rest of the analysis, staining, imaging, and all post-processing were done by me).

Permissive differentiation checkpoints in wound fibroblasts

Each stage of wound healing is intricately controlled and regulated by several molecular signals of mechanical and chemical origin. To grasp the connection between the divergence of $CD201^{+}$ fibroblasts and the related molecular cues, we dissected the role of seven related classical signals in our dataset of single-cell RNA sequencing (performed by Donovan). We found that the pathways inducing differentiation of fibroblasts into myofibroblast states included TGFβ, Wnt, and ECM mechano-transduction, all of which showed the most elevated level of action during the granulation and remodeling stages. Chemokines and other inflammation-related signals, on the other hand, were most prominent in the proinflammatory fibroblast state (figure 5a). This knowledge improved how we might interpret the unique way of interaction of these signals during the course of wound mending. During the transition from $CD201^{+}$ progenitors to proinflammatory fibroblasts, Donovan found that genes involved in the retinoic acid (RA) pathway show increased activity. Specifically, the enzymes Aldh1a3 and Rdh10, which are responsible for synthesizing RA, as well as the chemokines Ccl11, Ccl2, Ccl7, Ccl8, and Cxcl1, are found to be upregulated in proinflammatory fibroblasts derived from $CD201^{+}$ cells (figure 5b) which also corroborated in transgenic $CD201^{CreER}$ x $R26^{Ai14}$ animals (figure 5c-e). Additionally, the gene Cyp26b1 responsible for the degradation of RA was found to be overexpressed in proto-myofibroblasts located in the upper wound margins, where the differentiation process into myofibroblasts takes place (figure 5f) (the *in vivo* work with the animals and tamoxifen induction were supported by Donovan and all remaining post-processing and analysis were performed by me).

The link between fibroblast differentiation and RA signaling hints at the importance of spatial fibroblast differentiation in the wound dimension whereby a bottom-to-up direction was detected in relation to fibroblast progression of differentiation. To check the effects of extreme levels of RA (both high and low) in tissue repair, we again cultured ex vivo fascia tissue together with either the addition of extrinsic RA or an inhibitor that restricts RA expulsion in the tissue fraction. Both conditions increased the total RA signaling build-up around the tissue and reduced the contractile capacity of the explants significantly (figure 5g). This demonstrated the critical need for RA to be metabolized by the tissue at the right juncture of the healing

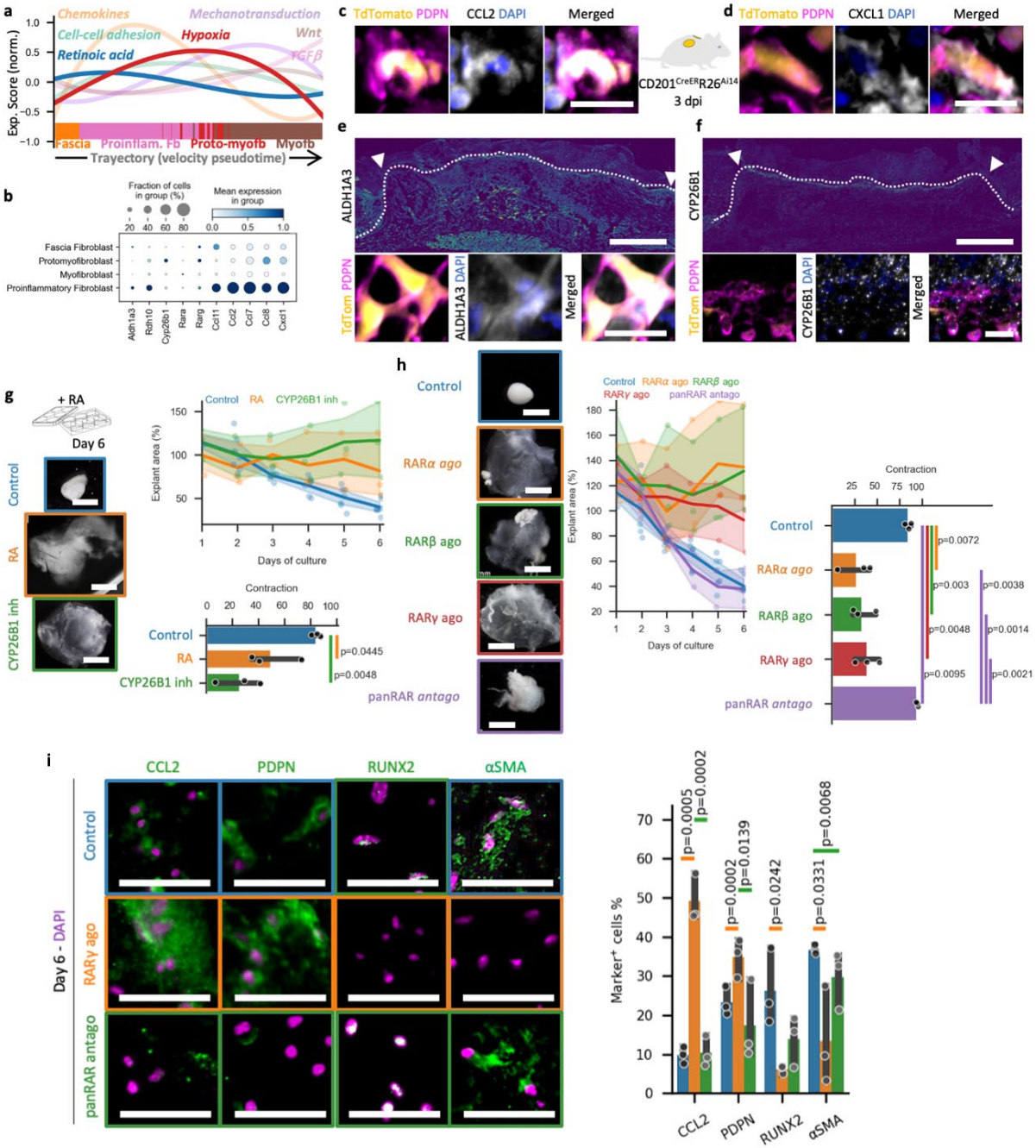

Figure 5 | The RA gate promotes an inflammatory state and inhibits myofibroblast differentiation. a. Fascia-to-myofibroblast differentiation routes combined with expression scores of classical molecular programs. **b.** RA-related genes and chemokine expression. **c, d.** High magnification images revealing PDPN and CCL2 (c) or CXCL1 (d) co-labelling in Cd201^{creER} x R26^{Ai14} line of lineage traced fascia fibroblasts. **e, f.** Top, to measure the quantity of expression '16_colours' pseudo-coloring was utilized in images stained with ALDH1A3 (e) and CYP26B1 (f). Bottom, higher magnification of the corresponding staining. **g.** Fascia explants were imaged under different conditions (control, RA-treated, and CYP26B1 inhibitor(inh) -treated) (left) to track tissue changes over a set period (top right) and quantify total shrinkage (bottom right. n = 3 biological repeats. The treatments in the graph are indicated by the colors of the picture outlines. **h.** Similar imaging and mathematical analysis on *ex vivo* fascia tissue with treatments with RAR-isotype inducers and pan-neutralizers together with their day-to-day photographs(left), area of shrinkage (middle) and total shrinkage (right). n = 3 (total contraction) and 4 (area vs time) biological repeats. **i.** High-mag images of control, RARγ inducer (ago) or pan-RAR neutralizer (antago) compounds stained for CCL2, PDPN, RUNX2 or αSMA (left) and their quantifications (right). The treatments in the graphs are indicated by the colors of the picture outlines. n = 3 biological repeats. Two-tailed Student's T-tests. Scale bars: 2 mm (g, h), 500 µm (e,f, top) and 50 µm (c, d, e & f bottom). Only figure panels e, f and illustrations a-b has been made by Donovan and modified from Correa-Gallegos, Ye, Dasgupta et al., Nature 2023 under Creative Commons Attribution 4.0 International License.

process in order to maintain the smooth progression of each stage. Similar experiments of treatments with the individual isotypes of the RA inducer showed a mirror effect of blocking contraction whereas a generalized RA neutralizer treatment enabled faster contractile maneuver thus indicating the impact of RA signaling is achieved through its conventional transcriptional routes (figure 5h). When tested for specific fibroblast subtype markers in these tissue fractions, we noted both PDPN and CCL2 protein expression were significantly higher in the RARγ inducing group, whereas the terminal differentiation markers for proto- and myofibroblasts like RUNX2 and αSMA were drastically reduced when compared to control tissue sections (figure 5i). This suggested that RA hyper activation restricts the differentiation trajectories and restrict fibroblasts in the proinflammatory state. The RA neutralized explants conspicuously didn't show any marked improvement in the ratio of proinflammatory to myofibroblast states implying the need for additional instructions to promote this final transition step (figure 5i).

We conducted another experiment where we cultivated $CD201^+$ fibroblasts in media containing wound signals that simulated differentiation (figure 6a). The proliferation-promoting medium only boosted the upregulation of SMA/Acta2, while the inflammatory-promoting medium amplified chemokines Ccl2 and Cxcl1 associated with proinflammatory differentiation (figure 6b). When RA was added to the inflammatory medium, the expression of PDPN and Ccl2 increased even more, while the expression of SMA/Acta2 and Cxcl1 decreased (figure 6c). Additionally, when RA was added to the proliferation medium, it resulted in a significant decrease in αSMA/Acta2 expression, which was consistent with the inhibitory effects of myofibroblast transition observed *ex vivo* (figure 6d). (These experiments were performed by Ruoxuan, Yue and Ravinder and were included to provide a comprehensive understanding of the topic and are adopted from Correa-Gallegos, Ye, Dasgupta, et al., Nature 2023).

Further investigation was conducted to assess the probable impact of RA overstimulation on the maintenance of the proinflammatory status and the resulting inflammatory phase in skin wounds. We utilized RARγ inducer in the treatment of these wounds. Despite not affecting the rate of wound healing (figure 6e), the application of the RARγ inducer to the subcutaneous region at 3 dpi resulted in more severe and prolonged inflammation in the treated wounds as evident through an increase in the presence of monocytes and macrophages within the wounds (figure 6f). Moreover, the RARγ treated wounds exhibited a noticeable decrease in αSMA^+ myofibroblasts at day 14 after injury, accompanied by the development of smaller scars. This

further supports the concept that in vivo RA activity contributes to the perpetuation of a proinflammatory fibroblast state (figure 6g). Furthermore, the excessive activation of RA inhibits the subsequent passage into contractile fibroblasts, ultimately leading to a reduction in scar development.

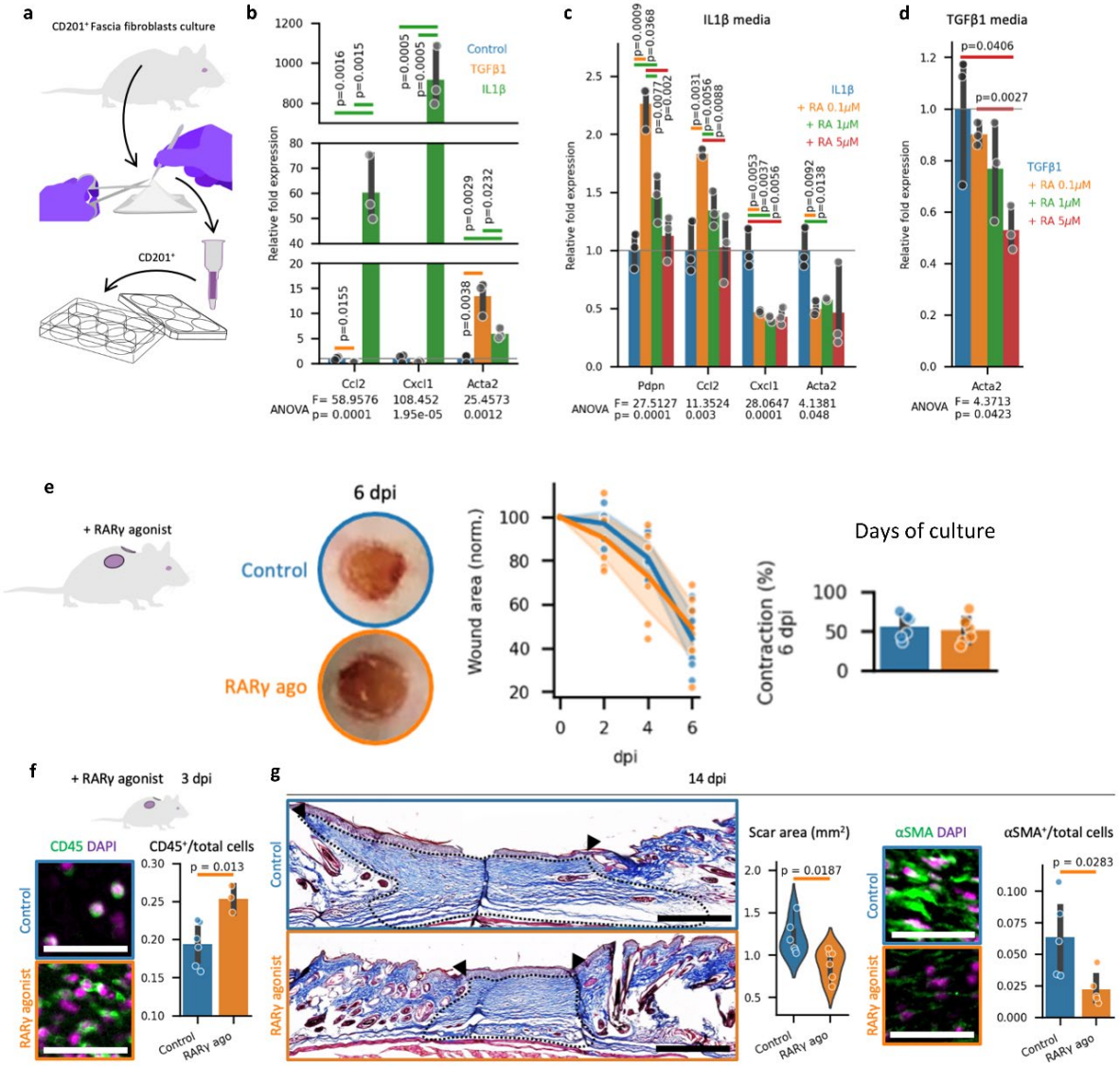

Figure 6 | RA fosters a tendency of hiring monocytes and cannot effectively facilitate further differentiation of fibroblasts. a. CD201$^+$ fascia cell enrichment and culture scheme. **b.** Relative fold change of Ccl2, Cxcl1 and Acta2 in control, L1β- (pro-inflammatory) or TGFβ1- (myofibroblast) conditioned treatments. n=3 technical repeats. Control values were used o normalize fold changes. Two-tailed student's T-tests (top) and one-way ANOVA (bottom) helped to generate p values etween the groups. **c-d.** Differential gene expression of relevant markers during inflammatory (c) and contractile (d) inducers ocultured with extrinsic RA at indicated concentrations. n=3 technical repeats. Control values were used to normalize fold changes. Two-tailed student's T-tests (top) and one-way ANOVA (bottom) helped to generate p values between the groups. **e.** Images of control or RARγ inducer-treated excision wounds at 6 dpi (left), wound area dimensions (middle), and total shrinkage at 6 dpi (right). 3 biological repeats generated n = 6 wounds. **f.** Staining of CD45, a pan-immune cell marker in control (top left) and RARγ inducer (top right) treated 3dpi wounds and their corresponding quantifications (right). The treatments in the graphs are indicated by the colors of the picture outlines. **g.** Overview images of Masson's trichrome stained control and control (top left) and RARγ inducer (top right) treated 14dpi wounds and their scar measurements (middle) from 3 biological repeats producing n=6 wounds per condition. The wound area is marked by dotted lines with arrows to depict the original injury location. High-magnification images of control (top right) and RARγ inducer (bottom right) treated wounds stained for myofibroblasts (αSMA) and quantified (extreme right). The treatments in the graphs are indicated by the colors of the picture outlines. 3 biological repeats generated n = 5 wounds. Two-tailed Student's T-tests. Scale bars: 500 μm (g left) and 50 μm (f left and g right). Only figure panels b-e have been made by Ruoxuan, Yue and Donovan and illustration a has been made by

Our findings collectively demonstrate that RA assumes a permissive function during the inflammatory stage of wound healing by fostering a phenotype that attracts monocytes and macrophages in proinflammatory fibroblasts derived from fascia. This is achieved through the expression of the monocyte chemoattractant CCL2. Even though an excessive activation of this route efficiently curtails the number of contractile fibroblasts, the downregulation of RA signaling alone does not suffice to initiate the shift into the myofibroblasts. Consequently, additional signals need to be present for this transition to occur.

Instructive checkpoint of fibroblast differentiation

Our *in-silico* analysis revealed that hypoxia holds an important role in the differentiation of fibroblasts along the wound trajectory and is positioned before the terminal differentiation step into myofibroblasts. It was seen that before the cells enter a more classical mechanism of TGF ß activation and mechano-transduction through YAP-TAZ pathway (Pakshir et al., 2020), there could an important role played by hypoxia to gate the transition of inflammation to granulation. More precisely, during the proinflammatory to proto-myofibroblast transition, the activity of hypoxia signaling through HIF1α gene is expressed innately and shown to be concurrent with progression of fibroblast differentiation (figure 7a) (illustrations created by Donovan). This observation was indeed corroborated in the $CD201^{+}$- and $PDPN^{+}$- lineage traced cells where we found $HIF1\alpha^{+}$ cells in the lineage positive cells to be colocalized and in fascia ex vivo tissue, all during the inflammation phase before differentiation into subsequent contractile states (figure 7b).

To expand our understanding on the exact role of hypoxia in the context of TGF ß signalling and why hypoxia is important for the proper progression of cell differentiation during wound healing course, Donovan further dug into the regulon expression of HIF1α gene against our inferred signalling activity. He found several central regulators like Pkm, Ddit4, En1, Eno1 and Ldha (Cho et al., 2021; Györfi et al., 2021; Judge et al., 2015; Xu et al., 2019; Zhang et al., 2021) and multiple peripheral regulators of TGFβ, Serpine1 and Lgals1(Gifford et al., 2021; You et al., 2021) that are upregulated in the proto- and myofibroblast clusters which led us to believe that the HIF1α functions upstream to both TGF ß and YAP/TAZ profiles (figure 7c-e).

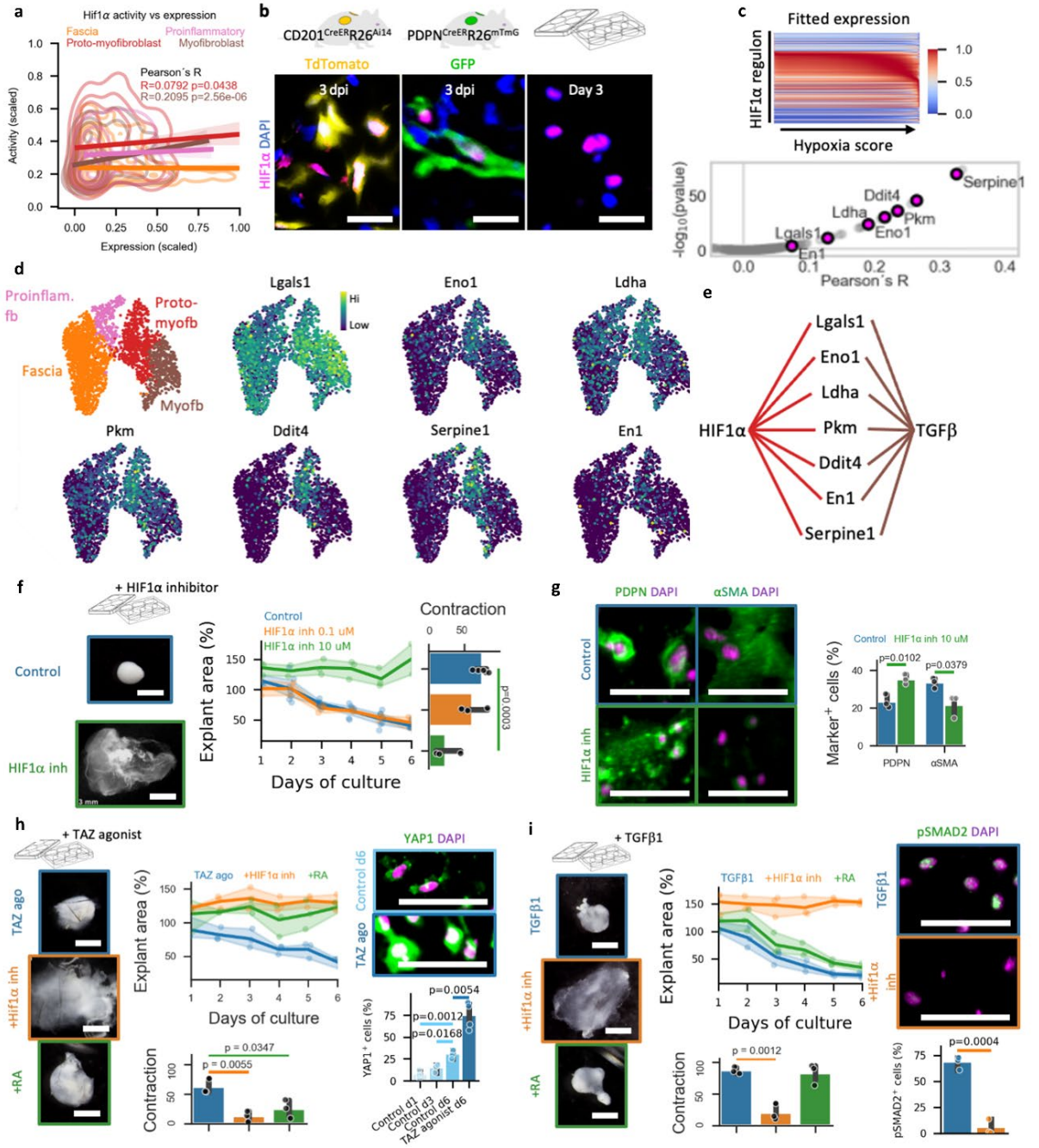

Figure 7 | HIF1 facilitates the move to proto-myofibroblasts. a. Pearson's R coefficient along with correlation of *in silico* HIF1α expression vs activity against fibroblast subtypes. **b.** High magnification images of HIF1α expression in 3dpi wounds or day6 on of ex vivo culture from indicated excision wounds or fascia explants. **c.** Expression of hypoxia score vs HIF1α regulon correlation (top) and genes that positively modulate TGF ß signaling (bottom). **d-e.** Graphics illustration of TGF ß modulatory genes and their involvement in the fascia trajectory. **f.** After 6 days of culture, control (left top) and HIF1 inhibitor-cocultured (left bottom) explants were measured for the area in the time course (middle) and shrinkage (right). N = 6 for the control and 3 for the inhibitor. g. Proinflammatory fibroblast (PDPN$^+$) or myofibroblast (αSMA$^+$) antibody labeling (left) and marker-positive fractions (right) in control (top) or inhibitor-treated (bottom) tissue samples. n = 3 biologic repeats. **h.** Coculture experiments of TAZ-inducing treatments (left top), together with inhibitors of HIF1α (left middle) and extrinsic RA (left bottom) with their measured area in the time course (middle top) and shrinkage (middle bottom). Corresponding staining for YAP1 (right top) and quantifications (right bottom) to show activation. n = 3 biologic repeats. **i.** Coculture experiments of TGF ß inducing treatments (left top), together with inhibitors of HIF1α (left middle) and extrinsic RA (left bottom) with their measured area in the time course (middle top) and shrinkage (middle bottom). Corresponding staining for pSMAD2 (right top) and quantifications (right bottom. n = 3 biologic repeats. The treatments in the graphs are indicated by the colors of the picture outlines. Two-tailed student's T-tests generated all p values (expect **a**) indicated on the bars. Scale bars: 2 mm in fascia tissue images (f-i) and 50 microns (b, g-i). Only illustrations a, c-e have been made by Donovan and modified from Correa-Gallegos, Ye, Dasgupta, et al., Nature 2023 under Creative Commons Attribution 4.0 International License.

Therefore, firstly we performed an experiment to inhibit the function of HIF1α in fascia explants and observe the effects its contractile ability and identify the cause of the alteration (created by Donovan). The contraction was indeed reduced in the treated samples in a dose-dependent manner (figure 7f) and αSMA^{+} terminally differentiated cells were seen to be reduced in numbers (figure 7g). On the other hand, $PDPN^{+}$ fibroblasts accumulated in a much higher number in the treated samples indicating that HIF1α inhibition was successful in restricting this specific transition between proinflammatory fibroblasts and myofibroblasts as indicated by our *in silico* data. HIF1α inhibition was key in blocking wound contraction even in the presence of classical modulators of tissue contraction such as YAP and TGF ß. Phospho-activated SMAD2 levels were also reduced in the HIF1α treatments that further confirmed nominal TGF ß activity in those cells (figure 7i). The addition of extrinsic RA together with YAP and TGF ß couldn't reproduce a similar phenotype, demonstrating a stronger action of HIF1α over RA signalling (figure 7h).

Inhibition of HIF1α *in vivo* through small molecule injection was performed by Haifeng and showed a delayed wound closure and poor matrix composition in the treatment group (figure 8 a-b) as also noticed in the proinflammatory lineage ablation experiment. On 3dpi, we also noticed no difference in the amount of immune cell infiltration in the wound area (figure 8c) which indicated HIF1α activity primarily regulates fibropblast, but not immune, differentiation. Furthermore, inhibiting Hif1α in $PDPN^{CreER}$ x $R26^{mTmG}$ wounds resulted in a substantial reduction in the number of proto-myofibroblasts and myofibroblasts of proinflammatory origin at 7dpi, providing further evidence of the crucial role of Hif1α in each of the differentiation step there on and ultimately on wound healing and scars (figure 8f).

In order to definitively illustrate the obligatory role of Hif1α in the process of myofibroblast differentiation during wound healing and its influence on the fibroblast subtypes, Donovan conducted experiments involving the use of Hif1α knockout mice in the context of fascia or proinflammatory fibroblasts (figure 8d). This was achieved by crossing both of our fascia $CD201^{CreER}$ and proinflammatory $PDPN^{CreER}$ mice with a strain containing loxP sites adjoining exon 2 of the Hif1α gene (Hif1aflox) which resulted in the knockout of Hif1α in specific fibroblast stages, through tamoxifen-induced recombination. Wounds inflicted on mice with a single allele omission in $CD201^{+}$ fascia ancestors exhibited similar wound closure characteristics as observed in wildtype mice, with no significant difference in wound size being closed by around 9dpi (figure 8d). Conversely, mice with bi-allelomorphic loss of Hif1α in

CD201^{+} fascia fibroblasts experienced a substantial delay in wound healing, with only 72.7% of the wound being closed at 9 dpi (figure 8d).

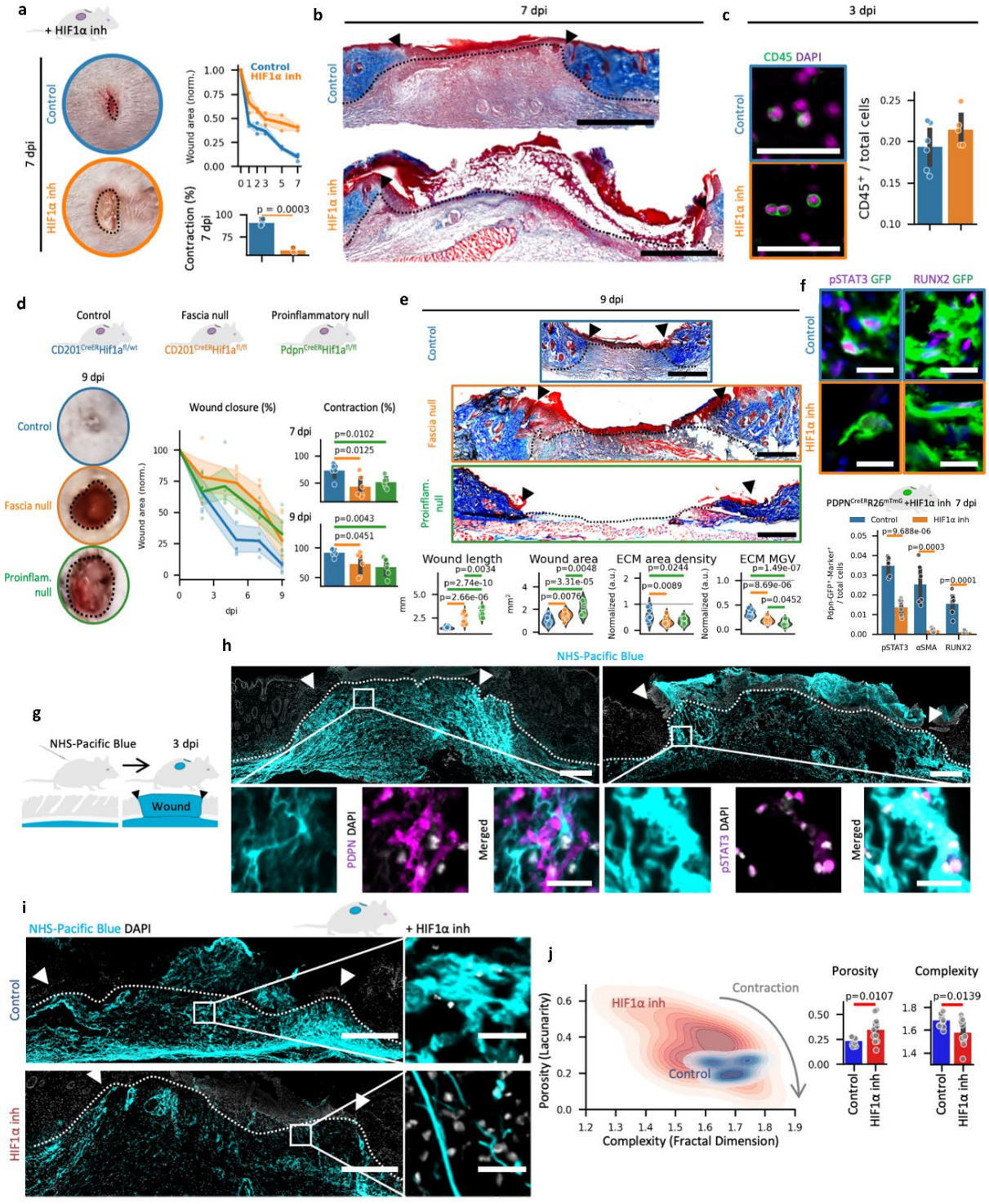

Figure 8 Inhibition of HIF1 limits progression of healing wounds. a. Pictures (left) of control (top) and inhibitor-treated (bottom) wounds at 7 dpi. Measurements of the wound's area over the course of time (top right) and overall shrinkage at 7 dpi (bottom right). n = 3 biological repeats. **b.** Masson's trichrome photographs of 7dpi control (top) and HIF1α treated (bottom) wounds. **c.** CD45 staining (left) and quantification (right) in control (top) and HIF1α treated (bottom) wounds at 3dpi. 3 biological repeats generated n = 6 (control) and 5 (treated) wounds. **d.** Brightfield photographs of control, fascia ane proinflammatory HIF1α deprived wounds (left), wound area dimensions (middle), and total shrinkage at 9 dpi (right). **e.** Trichrome micrographs (top) and wound evolvement-related values (bottom) of 9 dpi wounds from specified mouse lines. 3 biological repeats per line generated n = 6 wounds. **f.** Micrographs of PDPN^{creER} x R26^{mTmG} wounds with control and HIF1 inhibitor treatment displaying pSTAT3 or RUNX2 expression in GFP^{+} lineage cells (left) and positive cell fractions (right). 3 biological repeats per line generated n = 6 wounds. The treatments in the graphs are indicated by the colors of the picture

outlines. **g.** Graphic illustration to denote method of mapping the matrix. **h.** Overview (top) and expanded view (bottom) of control wounds examined with staining of PDPN or pSTAT3,to reveal a correlation with the architecture labelled ECM. **i.** Fascia extracellular matrix (ECM) was traced in 3-dpi wounds that were subjected to HIF1α inhibitor treatment. Low- (left) and high-magnification (right) images of both control (top) and HIF1α inhibitor-treated (bottom) wounds were captured. The wound areas are marked by dotted lines with arrows to depict the original injury location. **j.** Evaluation in porosity (lacunarity) and intricacy of shape (fractal dimension) was performed using lacunarity and the fractal dimension density plots inside the traced ECM of both control and HIF1α inhibitor-treated wounds (left), as well as distinct assessments (right). 3 biological repeats generated n = 11 images. Two-tailed student's T-tests generated all p values indicated on the bars. Scale bars: 500 μm (b, e, h top, i left) and 50 microns (c left, f top, h bottom, f and i right). Only figure panels a-b, d-e have been created by Haifeng and Donovan and illustration j has been made by Donovan and modified from Correa-Gallegos, Ye, Dasgupta et al., Nature 2023 under Creative Commons Attribution 4.0 International License.

Furthermore, delayed wound closure was also observed in $PDPN^{+}$ proinflammatory fibroblasts-Hif1α knockout mice ($PDPN^{CreER}$ x $Hif1a^{fl/fl}$), with only 62.5% of the wound being closed at 9 dpi. The wound development was also immature in both the genetic deletion models akin to the PDPN ablation wounds and couldn't propagate normal wound closure phenotypes as observed in control groups (figure 8e). These observations thus uncovered the direct relevance of Hif1α in the transition of $PDPN^{+}$ proinflammatory fibroblasts to terminal myofibroblast state and thereby affecting development of scars.

In an earlier study we described the importance of mobilized fascia connective tissue in skin wound repairs (Correa-Gallegos et al., 2019). To investigate the impact of the transition from proinflammatory fibroblasts to remodeling and collagen producing states on ECM modulation, we labelled the fascia ECM using an NHS-ester dye that binds to the positively charged lysine residues of the fascia ECM fragments, by injecting the chemical subcutaneously (figure 8g). At 3dpi, we found that labelled fascia ECM entered and encompassed almost every region of the wound area. Looking closely, we found that the architecture of ECM fibers corresponded to the mode of the action undertaken by specific fibroblasts subtypes. The light and sparsely allocated fibers were incorporated around the $PDPN^{+}$ proinflammatory fibroblasts whereas the tightly bound, closely webbed fibre knits were covered with $pSTAT3^{+}$ proto-myofibroblasts (figure 8h).

These results support the idea that the transformation of $CD201^{+}$ progenitors into ECM-modulating fibroblasts, such as proto- and myofibroblasts, played a role in the flexibility of the matrix and the contraction of the connective tissue. To delve deeper into this hypothesis, we injected the Hif1α inhibitor in animals with labelled fascia ECM to block the differentiation into proto- and myofibroblasts (figure 8i). In comparison to the control group, the wounds in the treated animals at 3dpi displayed a more loosely organized and fragile arrangement of fibres, indicating that inhibiting the differentiation of proto- and myofibroblasts led to a less

condensed fibre organization. Donovan then performed fractal analysis on these experimental groups to identify the differences in the matrix composition and networking in the control and treated wounds. The Hif1-inhibition group was severely outperformed by the controls in terms of complexity and they also had much higher porosity compared to controls (figure 8j). This provided additional support for the hypothesis that a relaxed fibre organization was achieved by inhibiting differentiation into proto- and myofibroblasts.

In conclusion, our *in-silico* analysis, *in vivo* and *ex vivo* experiments, together with small molecule inhibition, multiple gene modulating procedures and ECM tracing outcomes all point to the fact that, in mice, an instructive signaling through Hif1α is pivotal for the transition between proinflammatory and proto-/myo fibroblast stages during progression of healing wounds.

Translation in human physiology

To discover if the sequential transition of fibroblasts is ubiquitous among humans as well, $PDGFRA^{+}$ cells from many injury conditions where myofibroblast activity are pronounced were merged. The annotations discovered in the mouse dataset were then applied to this merged human data using transfer learning strategies (figure 9a-b). The data was exclusively and comprehensively generated by Donovan with support from Safwen Kadri and can be found detailed in our published paper Correa-Gallegos, Ye, Dasgupta, et al., Nature 2023. As a summary, different populations of proinflammatory fibroblasts, proto-myofibroblasts, and myofibroblast-like cells were observed in various human skin pathologies, alongside three resident populations involved in maintaining skin homeostasis. The composition of fibroblasts also varied between different skin diseases, with progenitor fibroblasts being more widespread in hypertrophic scars and papillary fibroblasts being more regular in scleroderma situations. Inflammatory fibroblasts and contractile fibroblasts were available in all circumstances, but pro-inflammatory subtypes were mostly visible in keloids and scleroderma, while the contractile fibroblasts were more abundant in psoriatic skin (figure 9c). Proto-myofibroblasts, however, were only found in hypertrophic scars and psoriatic skin datasets. Comparative analysis of specific markers in human fibroblast clusters and their mice equivalents revealed

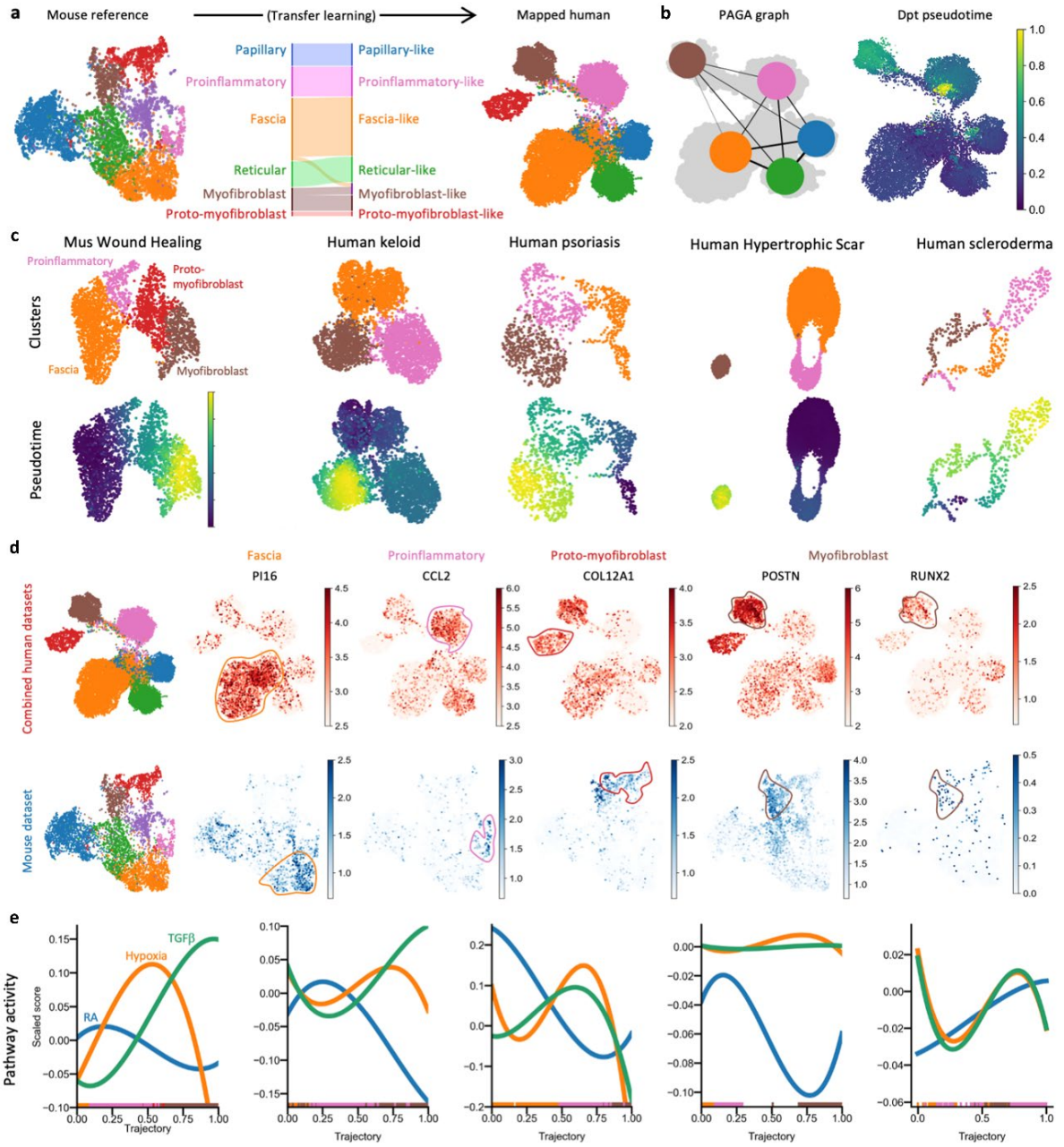

Figure 9 | Fibroblast differentiation in human skin diseases. a. Human fibroblasts were mapped from mouse database using Transfer learning' strategies and their corresponding UMAPs. **b.** PAGA associated links overlayed on fibroblast UMAPs (left) and their pseudotime diffusion score. **c.** UMAP investigations (top) and their values in pseudotime (bottom) of human skin diseases with fibroblast subclusters of in mouse wound healing as reference showed that fascia fibroblasts must transition to proinflammatory fibroblasts before becoming myofibroblasts. **d.** UMAP visualizations show conserved marker is expression cross the combined mouse (top) and human (bottom) datasets. **e.** Consistent links between RA and the proinflammatory state and hypoxia and the myofibroblast state were revealed in the molecular programs of RA, hypoxia, and TGFβ across all datasets. All illustrations have been made by Donovan & Safwen and modified from Correa-Gallegos, Ye, Dasgupta, et al., Nature 2023 under Creative Commons Attribution 4.0 International License.

several conserved markers. Pi16 was identified as the most specific marker for the fascia clusters in both human and mouse datasets (figure 9d). Interestingly, the presence of RUNX2, a marker not traditionally associated with myofibroblasts, was confirmed in keloid lesions but not in healthy tissue. The study also demonstrated that homeostatic and wound fibroblasts in mice share similarities with human fibroblasts. Analysis of the trajectory unveiled enhanced

networking within all homeostatic cell types and their passage into the proinflammatory and contractile fibroblast subtypes as the last differentiation stage. This suggests that the homeostatic populations contribute differently to the group of wound fibroblasts.

We discovered that human fascia fibroblasts undergo a transformation into myofibroblasts by means of a proinflammatory condition, which is comparable to the wound healing process in mice and similarly, this is hindered in skin disorders. The conservation of the two signalling gates, RA and hypoxia, was also examined. It was observed that RA activity reaches its highest point during the proinflammatory state in all diseases, except for psoriatic skin. Furthermore, the activity of the hypoxia signal was found to be correlated with the TGFβ signalling pathway (figure 9e). Our analysis shows that human fascia fibroblasts differentiate into proinflammatory fibroblasts and contractile myofibroblasts, influenced by RA signalling and Hif1α-mediated hypoxia signal, significantly impacting wound healing progression.

Discussion

Our research sheds light on a remarkable and unchanging differentiation process. This process holds tremendous clinical significance, particularly when it comes to wound healing. The core of this process revolves around the emergence of fascia progenitors, which serve as the foundation for the development of distinct fibroblast types. In addition to this pivotal role, these fascinating progenitors also play a crucial role in establishing two regulatory gates. These gates serve as critical checkpoints, ensuring that the wound healing phases progress in a timely and efficient manner. These findings carry significant implications that have the potential to completely transform our approach to and treatment of injuries.

It is crucial to emphasize that the initial transformation of fascia progenitors into proinflammatory fibroblasts plays a vital role in the inflammatory phase. The research findings shed light on the involvement of RA (retinoic acid) in supporting this particular phase. Specifically, RA sponsors a phenotype that has the capability to attract monocytes, while at the same time forestalling their transformation into myofibroblasts. It also explains why the effects of RA cannot override the classic TGFß and YAP/TAZ signals in the end as it can only stall the cellular differentiation and help in the maintenance of the inflammation state. Consequently, this mechanism effectively provides an explanation for the observed anti-fibrotic effects of exogenous RA (Phan et al., 2021).

The second phase of differentiation is of utmost importance due to its involvement in the shift from proinflammatory to (proto-)myofibroblasts. This change is described by the procurement of a phenotype in its contractile nature, which serves a pivotal role in the transition to the subsequent proliferation and remodeling periods of healing wounds from the existing

inflammatory phase. Previous investigations have placed significant emphasis on Hif1α in fibroblasts for the timely and efficient healing of wounds (Duscher et al., 2015). In addition to its well-established functions in the clearance of reactive oxygen species and the regulation of angiogenesis, our gathered data offers direct evidence supporting the notion that Hif1α possesses an upstream regulatory role in the TGFβ pathway (Zhao et al., 2017). This regulatory influence indirectly impacts the transition towards myofibroblasts, thus highlighting the intricate and interconnected nature of the wound healing process.

Until now, a lot of focus has been given towards myofibroblasts and their spatial location in wounds with most of them directed to point at the upper halves of the injury area. Minimal attention has come to the deeper areas of wounds until now due to the lack of a clear understanding of the dynamics in that region. The role of fibroblasts in wound healing has always been well vetted over several decades but still very little stress has been given to specific subtypes of fibroblasts that perform distinct designated roles in the course of healing wounds. We have looked into this specific aspect very closely by compartmentalizing the role of distinct population according to their spatial and temporal location on relevant days of injury repair and identified a progenitor population in the deep lying fascia connective tissue of skin. These population, termed as $CD201^{+}$ fascia fibroblasts, have displayed an ability to differentiate sequentially into distinct role bearing fibroblast cells in a bottom to top spatial direction under the influence of specific molecular cues during wound healing.

The initial instruction takes place in the area of the wound where specialized cells mature to proinflammatory fibroblasts and the Retinoic acid cues are at its peak. The next subsequent molecular cue arises within the inner wound area comprising of poor oxygen supply as a natural response to hypoxia in proinflammatory fibroblasts. The interplay of both these signals,

reminiscent of a carefully choreographed symphony, orchestrates the gradual evolution of cells into proto-myofibroblasts but due to sustained presence of the RA molecular cue these cells are unable to progress further into the subsequent differentiation states in the wound area. This is bypassed slightly later when RA is finally metabolized in the upper areas of the wound as the cellular transition progresses, that the cells can finally differentiate into their final contractile state of becoming $RUNX2^{+}$ and αSMA^{+} myofibroblasts. Therefore, evidence from our study indicates an intricate interplay between RA gradients within the depths of hypoxic niches. It is in these space that the orchestration of fibroblast differentiation unfolds, driven by injury phenotype.

The findings of this study have significant clinical implications, as disruptions in the process of cellular differentiation can lead to various pathologies, including impaired wound healing and fibrotic scarring. In particular, the ability to manipulate specific actions down this route initiates new avenues for tailoring therapeutic interventions for different types of wound fibroblasts. By carefully modulating these cells, it may be possible to develop targeted therapies that address the underlying disease processes. For example, treatments for wounds resulting from surgical procedures, keloids, burns, and other injuries may possibly be engineered to limit the activation of myofibroblasts, thereby blocking unnecessary collagen deposition and tissue contraction. Importantly, this approach would not negotiate with the crucial proinflammatory function of these cells during the initial inflammation of wound healing stages. In parallel, treatments designed to transform the behaviour of early progenitor cells could significantly benefit individuals suffering from skin ailments of inflammatory origin.

Material and methods

Mice and genotyping

Jackson Laboratories or Charles River provided us with B6. Cg-Gt(ROSA)26Sortm14(CAG-tdTomato) Hze/J ($R26^{Ai14}$), B6.129 (Cg)-Gt(ROSA)26Sortm4(ACTB-tdTomato.-EGFP)Luo/J ($R26^{mTmG}$), C57BL/6J wildtype, En1tm2(cre) Wrst/J ($En1^{Cre}$), and B6.129S6(Cg)-Gt(ROSA)26Sortm1(DTA)Jpmb/J ($R26^{DTA}$) strains of mice. $PDPN^{CreER}$ line was produced internally, and Dr. Ariel Zeng (SIBCB) presented us with the CD201/ $Procr^{CreER}$ line. The Institute of Diabetes and Obesity (IDO) gifted us B6.129-Hif1atm3Rsjo/J ($Hif1a^{flox}$) animals from the Helmholtz Centre Munich. Helmholtz Central Animal Facility housed all the animals; cages are kept warm and humid with a 12-hour photoperiod, and food and water are provided *ad libitum*. All animal tests were checked on and endorsed by the Upper Bavarian state government and enrolled beneath ventures 55.2-2532-02-19-23 and 55.2-1-54-2532-16-61 together with strict government and international rule and the entire study complies with all pertinent moral directions with respect to animal research. Animal experiments were performed using 8- to 12-week-old adult mice. Important genotypes were recognized by standard PCR and gel electrophoresis. To do this, the manufacturer's instructions for the Quick Extract DNA extraction solution (Epicentre) were followed to extract the genomic DNA from the earclips. For every 19 µl PCR reaction, 1µl of DNA extract was added. The reaction mixture was created with the GoTaq PCR core kit (Promega), which included 1x GoTaq green master mix and 0.5M forward and reverse primers. The primers that were used are depicted in Table 1. Sigma Aldrich supplied all the primers. PCRs were run for 5 minutes at 94 °C, followed by 35 cycles of amplification (denaturation for 30 seconds at 94 °C, hybridization for 30 seconds at 59 °C, and elongation for 1 minute at 72 °C), and then cooled to 4 °C. Negative controls (non-template and extraction) and positive controls were included in each run. The reactions took place on an

Eppendorf master cycler. Electrophoresis in agarose gels was used to detect amplified bands. Other mouse lines (mTmG, Ai14, and DTA) were kept in a homozygous state.

Primer name	Sequence
PDPN-Cre-FW	5'-gatggggaacagggcaagttgg-3'
PDPN-Cre-RV	5'-ggctctacttcatcgcattccttgc-3'
Hif1a-FW	5'-tgcatgtgtatgggtgttttg-3'
Hif1a-RV	5'-gaaaactgtctgtaacttcatttcc-3
En1-Cre-FW	5'-attgctgtcacttggtcgtggc-3'
En1-Cre-RV	5'-ggaaaatgcttctgtccgtttgc-3'
Procr-Cre-FW	5′-gcggtctggcagtaaaaactatc-3′
Procr-Cre-RV	5′-gtgaaacagcattgctgtcactt-3

Table 1 | List of primers used for genotyping

Excision wound models, Tamoxifen supplementation and Compound treatments

For descriptive experiments, both male and female mice, equally distributed across time groups, were used. Animals of the same litter or age were randomly assigned to the various experimental groups for functional studies. To diminish fluctuation, just males were utilized for the RARγ agonist and Hif1α restraint medicines (7 dpi), and for the Hif1α hereditary cancellation explore. For both 3 dpi $PDPN^{+}$ cell ablation investigations and the 3 dpi Hif1 inhibition study, equal numbers of females and males were used. Spine full-thickness wounds were conducted on mature (8–12-week-old) mice as previously described (Correa-Gallegos et

al., 2019). In brief, bilateral 5 mm circular wounds were made by piercing a skin fold along the midline of the back using biopsy punches (Stiefel 10005). Immediately after the excision wound was made for splint wound model (Dunn et al., 2013), a circular silicone ring was glued (Gracebio 664581) and stitched around the open wound. $CD201^{CreER}Hif1a^{fl/wt}$, $CD201^{CreER}Hif1a^{fl/fl}$, $CD201^{CreER}R26^{Ai14}$, and $PDPN^{CreER}Hif1a^{fl/fl}$ mice for genetic lineage tracking of $CD201^{+}$ fascia fibroblasts and HIF1a gene deletions 2 mg (Z)-4-hydroxytamoxyphene (Sigma Aldrich H7904) 0.2ml (caesar& it was analyzed using lorentz gmbh). CSLO3274) two days and one day before the injury and the day of the injury. For genetic lineage tracking and ablation of $PDPN^{+}$ inflammatory fibroblasts, $PDPN^{CreER}R26^{DTA}$ or $PDPN^{CreER}R26^{mTmG}$ mice received daily intraperitoneal injections diluted with 1 mg (Z)-4-hydroxytamoxifene 0.1ml migliol-812 from the fourth day before the day of injury. 40 µl 2 mg/ml Pacific Blue succinimidyl Ester (Invitrogen P10163) was injected subcutaneously along with with 0.1 M sodium bicarbonate in saline for fascia matrix fate mapping(Correa-Gallegos et al., 2019; Fischer et al., 2023). Hif1a inhibitor (echinomycin, Sigma Aldrich sml 0477), a RARγ agonist (BMS 961, Tocris 3410), a 100 µg / Kg body weight concentration or a vehicle control dimethyl sulfoxide (DMSO, Sigma Aldrich D5879) were administered near or under the wounded area on alternate days at a concentration of 100 µg / Kg body weight to have a sustaining effect on fibroblasts.

Ex-vivo fascia culture system

Using scissors and forceps, the back skin of the deceased mice was carefully removed, taking great care to preserve the underlying fascia. The fascia, which is the connective tissue beneath the skin, was crucial to the experiment and needed to remain intact. After the skin was removed, the samples were washed twice in ice-cold PBS (Phosphate Buffered Saline) from Thermo Fischer. This step was important to eliminate any residual debris or contaminants that could

interfere with the experiment. Once the samples were cleaned, they were positioned with the epidermal side facing downwards. This ensured that the fascia was easily accessible for further manipulation. The soft fascia tissue was then gently pulled and roughly cut into 4 mm fragments using forceps. This step was necessary to create smaller, manageable pieces of tissue for the experiment. The forceps were used to carefully handle the tissue and prevent any damage. After the fragments were cut, they were thoroughly cleaned again in PBS. This ensured that any remaining debris or contaminants were removed, further preparing the tissue for the experiment. Finally, the cleaned fascia explants were placed in triplicate within 6-well plates. Placing the fascia explants in triplicate allowed for multiple replicates of the experiment, increasing the reliability of the results. These plates contained a culture medium commonly used for cell and tissue culture DMEM/F-12 with 10% normal FBS or heat-inactivated FBS (BioConcept, 2-02F110-I; heat inactivated at 56°C for 30 minutes), or 0.5% low serum concentrations, 1x GlutaMAX (Thermo Fisher Scientific 35050038), 1x penicillin/streptomycin (Thermo Fisher Scientific 15140122), and1X MEM non-essential amino acids (Thermo Fisher Scientific 11140035). Every two days, the media were changed. During the ex vivo cell ablation process, the cells underwent three cycles of freezing for one hour at -80°C, followed by thawing for 30 minutes at room temperature. This freezing and thawing process was necessary to ablate the cells and prepare them for culturing. During the change of media, the media in the treatment groups was refreshed and enriched with additional compounds. The composites used include the RARγ agonist (0.01 μM, BMS 961, Tocris 3410), CYP26B1 inhibitor (0.01 μM, R115866, Sigma Aldrich SML2092), Hif1α inhibitor (0.1, 10 μM, echinomycin, Sigma Aldrich sml0477), RA (0.01 and 1 μM, R&D systems 0695), panRAR antagonist (0.01 μM, AGN193109, Tocris 5758), RARα agonist (0.01 μM, AM580, Tocris 0760), RARβ agonist (0.01 μM, CD2314, Tocris 3824), TGFβ1 (10 μM, recombinant mouse TGF-beta 1 protein, R&D systems 7666-MB-005/CF), and TAZ agonist (10 μM,

Kaempferol, R&D systems 3603/50). The Hif1 inhibitor and RA effective doses for the combined treatments were 10 and 1 mM, respectively. The samples were carefully stored in a specialized humidified incubator set at a constant temperature of 37 °C. Additionally, the incubator was enriched with 5% CO2 to create an optimal environment for the samples' preservation. For mouse samples, the maximum duration of storage was set at six days. These time limits were determined based on previous research and experimentation, ensuring that the samples remained viable and suitable for further analysis. To monitor and assess the contraction of the fascia tissue, a daily imaging process was implemented. This involved utilizing a Leica M50 stereomicroscope, a high-quality imaging instrument known for its precision and clarity. The stereomicroscope allowed for detailed visualization of the samples, to observe any changes or contractions in the fascia tissue over time.

Sections and Immunohistochemistry

At the appropriate intervals, the samples were fixed with 4% paraformaldehyde (PFA, VWR 43368.9M) for an entire night before being processed for cryosectioning in a Cryostat (CryoStar NX70) with an OCT (CellPath KMA-0100-00A). To prepare the sections for immunostaining, they were blocked for one hour at room temperature using a blocking solution containing 10% serum in PBST. Prior to blocking, the sections were rinsed three times with PBST solution (PBS containing 0.05% Tween). For immunostaining, the sections were incubated with the primary antibody for three hours at room temperature or overnight at 4 °C in blocking buffer. After incubation, the sections were rinsed three times with PBST for 5 minutes each. Next, the sections were incubated for 60 minutes at room temperature with the appropriate secondary antibody in blocking solution. Following this incubation, the sections were rinsed three times in PBST for 5 minutes each. Finally, the sections were mounted using fluorescent mounting media containing 4,6-diamidino-2-phenylindole (DAPI). The fixed

fascia samples, which were approximately 1cm^2 in size, were placed in a solution of PBSGT that contained 0.2% Gelatine (Sigma G1393), 0.5% Triton X-100 (Sigma X100), and 0.01% Thimerosal (Sigma T5125). These samples were incubated in this solution for a period of 24 hours. After the initial incubation, the samples were then incubated at room temperature for 48 hours with the primary antibody in PBSGT. The primary antibodies used in this study are listed in Table 2. Following the primary antibody incubation, the samples were incubated for a minimum of 48 hours or until imaging with the relevant secondary antibody for the species in PBSGT. The secondary antibodies used were AlexaFluor488-, AlexaFluor568-, or AlexaFluor647-conjugated secondary antibodies, which were diluted at a ratio of 1:500 (Life Technologies). For certain primary antibodies, such as pSTAT3, RUNX2, and HIF1A, antigen retrieval was performed using citrate buffer at 80 °C for 30 minutes. After the antigen retrieval step, the samples were allowed to cool for 30 minutes before proceeding to the blocking step. Against the respective species, AlexaFluor488-, AlexaFluor568-, or AlexaFluor647-conjugated secondary antibodies (1:500 dilution, Life Technologies) were utilized. Masson's trichrome staining procedure is a widely used histological technique that allows for the visualization of collagen fibers, muscle fibers, and other connective tissues in tissue sections. In this study, a commercial kit from Sigma Aldrich (HT15) was used to perform the staining procedure according to the manufacturer's instructions. Histological sections were prepared and stained using Masson's trichrome staining kit. The sections were then examined and captured using two different microscopes. The first microscope used was a ZEISS AxioImager. Z2m microscope equipped with a 20x objective. This microscope provides high-resolution images and is commonly used for histological analysis. The second microscope used for imaging was the THUNDER Imager Model Organism from Leica. This microscope also had a 20x compiled zoom capability, allowing for detailed examination of the stained sections. The THUNDER Imager Model Organism is specifically designed for imaging biological samples

and provides enhanced resolution and contrast. In addition to the sectioned samples, whole-mount samples were also imaged using a Leica SP8 Multiphoton microscope. This microscope utilizes multiphoton excitation to capture high-resolution images of thick samples, such as whole-mount tissues. The Leica SP8 Multiphoton microscope is equipped with advanced imaging capabilities, including spectral detection and high-speed scanning, making it suitable for imaging complex biological samples.

Image Quantifications

Fiji (v.1.53c) was used for all image analysis. Using the "Selection Brush" tool and the "Measure" function, the explant or wound area from various timepoints was selected for evaluation of tissue contraction in vitro and wound closure in vivo. The initial (day 0, A0) percentage of area values was normalized to 100%. The difference between the highest area value from the first two days of culture (day 0-2, Amax) and the lowest area value from the last two days of culture (day 4-6, Amin) was used to calculate in vitro final contraction (C). in this way, C = Amax-Amin. Using a line measurement tool, lines were traced along the new epidermis, the distance between flanking hair follicles, and the distance between the branched Panniculus carnosus muscle in each section to calculate the mean length of the wound. The functions "Subtract Background" (rolling=20px), "Median" (radius=1), "Unsharp Mask" (radius=1, mask=0.60), "Despeckle," "Enhance Contrast" (saturated=0.1 normalize), and "Auto Threshold" were used to pre-process individual channels for cell marker positive quantifications: " Moments, Intermodes (RUNX2, TdTomato, PDGFR, and LYVE1), Yen (CCL2), IsoData (PDPN), or RenyiEntropy (SMA) (for DAPI, pSTAT3, YAP1, pSMAD2, CD45, and GFP signal). Using the "Selection Brush" tool, the wound region of interest (ROI) was manually selected using the breached Panniculus carnosus below the dermis and the adjacent epidermal hair follicles above.

Name of Antibody	Company and Catalog No.	Dilution Used
LYVE1	Abcam ab14917	1:100
αSMA	Abcam ab21027	1:150
YAP1	Abcam ab205270	1:100
pSMAD2	Cell Signalling 18338	1:100
CCL2	Abcam ab25124	1:100
CXCL1	R&D systems MAB453R	1:100
PDPN	Abcam ab11936	1:500
RUNX2	Abcam ab92336	1:150
pSTAT3	Cell Signaling 9145S	1:150
CYP26B1	Elabscience E-AB-36196	1:100
ALDH1A3	Novus NBP2-15339	1:100
Pi16	R&D systems AF4929	1:100
CD45/PTPRC	Abcam ab23910	1:100
PECAM1/CD31	Abcam ab56299	1:50
KRT14	Abcam ab181595	1:100
PDGFRα	R&D systems AF1062	1:100
GFP	Abcam ab13970	1:500
HIF1A	Novus NB100-479	1:100

Table 2 | List of Primary antibodies used

The DAPI channel and the functions "Fill Holes," "Watershed," and "Analyze Particles" (size=70-1400px) were used to measure the total number of wound cells within the ROI of binary images. The DAPI channel's "Image Calculator_AND," "Dilate" twice, "Close," "Fill Holes," "Watershed," and "Analyze Particles" functions (size=70-1400px) were used to measure the marker's positive cell numbers. An initial mask made from two marker channels

was created and processed as before for double marker positive cell calculations. The "Selection Brush" tool was used to manually select three ROIs for wound region quantification. The upper wound region extended vertically 200 microns from the wound surface (at 3 dpi) or the wound epidermis (at 7 dpi), delineating the wound's lateral limits. The wound core covered the space in between the wound fascia and the upper wound, while the area below the breached P. carnosus muscle and down to the dorsal muscles was measured as the fascia. The ROIs were cleared of non-mesenchymal areas like wound epidermis and hair follicles. The "Measure" function was used to determine the Mean Gray Value (MGV) for each ROI after the marker channels were processed as before. For visual guide, marker signal power was addressed with the "Fire" or "16-variety" pseudo-colors. The RGB-to-CMYK plug-in was used to convert Masson's Trichrome Stained RGB images into CMYK for the purpose of determining the ECM area density. Then, the cyan channel (ECM) was separated and the MGV estimated prior to being pre-handled as above. The ECM (cyan) area in the wound that covered the entire wound was what was used to define ECM density. To avoid batch effects between stained sections, wound ECM density and ECM MGV were normalized to the healthy dermis adjacent to the wound. As before(Ascensión et al., 2021), fractal analysis was carried out. Momentarily, the Cyan channel was pre-handled as in the past, and paired pictures were produced utilizing "Auto Edge" ("Default" technique) capability. Paired pictures were then investigated with the FracLac module involving similar settings as in the past. Seaborn and Matplotlib, both of which are based on Python, were used to create all of the quantification plots.

Stromal cell enhancement for scRNAseq

During the critical stages of injury, we collected samples of 8 mm-diameter wounds and the surrounding skin from En1CreR26mTmG dorsal skin wounds. To ensure accuracy, we combined three samples from six wounds at each time point. The collected tissue was then minced using surgical scissors and digested for 60 minutes at 37°C using the Liberase TM enzymatic cocktail supplemented with 25 U/ml DNase I (Sigma Aldrich D4263). After digestion, the tissue was filtered to obtain a single cell suspension. The single cell suspension was then incubated with conjugated primary antibodies (dilution 1:200) against specific cell markers of undesirable cell type lineages for 30 minutes at 4 degrees Celsius. Some of the antibodies used included APC-anti-CD31 (eBioscience 17-0311-82), eFluor660-anti-Lyve1 (eBioscience 50-0443-82), APC-anti-Ter119 (Biolegend bld-116212), and APC-anti-CD45 (Biolegend Bld-103112). After incubation, the cells were washed and incubated at 4° C for 20 minutes with appropriate fluorescent markers and dead cell markers (Dead Cell evacuation unit, Miltenyi 130-090-101).

For cell isolation, we used OctoMACS and MS segments (Myltenyi) following the manufacturer's guidelines. Negative selection was performed to isolate the desired cells, and the cells were then washed, counted, and diluted in PBS with 300 U/ml of RNase inhibitor (RiboLock LIFE technologies eo0382) at a concentration of 100 cells per microliter. Only samples with more than 90% living cells were used for Dropseq separation.

S*equencing after dropseq library arrangement*

The analysis and sequencing were performed according to Correa-Gallegos, Ye, Dasgupta et al., Nature 2023 and are outlined here. In this study, stromal-enriched cell suspensions were isolated using a microfluidic-based technique called Dropseq52. The protocol used was based on the one developed by the McCaroll lab, with a few modifications. First, cells were

encapsulated in droplets along with barcoded beads from ChemGenes Corporation. This was done using a microfluidic PDMS device called Nanoshift, with a flow rate of 4000 µl/hr. The droplet emulsions were collected for 15 minutes each before breaking the droplets using perfluoro-octanol from Sigma-Aldrich. After droplet breakage, the barcoded beads were collected and the mRNA transcripts from the cells were reverse transcribed using Maxima RT from Thermo Fisher. Excess primers were removed using exonuclease I from New England Biolabs. The beads were then washed, counted, and divided into aliquots for pre-amplification. Each pre-amplification reaction contained 2000 beads, which represented approximately 100 cells. The pre-amplification was done with 12 PCR cycles using the recommended settings. The PCR products from the pre-amplification reactions were combined and purified twice using 0.6x clean-up beads from CleanNA. Before tagmentation, the cDNA samples were analyzed on a DNA High Sensitivity Chip on the 2100 Bioanalyzer from Agilent to ensure the integrity, purity, and quantity of the transcripts. For tagmentation, 1 ng of pre-amplified cDNA from each sample, which represented an estimated 1000 cells, was used. The tagmentation was done using Nextera XT from Illumina, with a custom P5 primer from Integrated DNA Technologies. The single cell libraries were then sequenced in a 100 bp paired end run on an Illumina HiSeq4000. The sequencing was done using 0.2 nM denatured sample and 5% PhiX spike-in. For the 1st read, priming was done using 0.5 µM Read1CustSeqB primer. Finally, the reads obtained from the sequencing were mapped and aligned to the mm10 genome reference, which was provided by the Drop-seq group (GSE63269). This genome reference was customized to include the eGFP cDNA transcript. The mapping and alignment were done using STAR version 2.5.2a.

Analysis of scRNAseq data

The Scanpy53 python toolkit and its associated tools within its ecosystem were utilized to conduct all the analyses. The matrices of individual samples were merged and underwent quality control measures, which included filtering out cells with a gene count below 100.Almost all the analyses were performed majorly by my colleague Donovan Correa-Gallegos and the details are indicated in the published paper. The initial alignment was supported by Meshal Ansari, Ilias and Hert Schiller as also indicated in our paper (Correa-Gallegos, Ye, Dasgupta et al., Nature 2023).

Statistics

Python toolkit Scipy was utilized for the statistical analysis. In a typical setting, Two-tailed T-test, 1- or 2-way ANOVAs, and Pearson's R were used. A significant difference is considered If the P value is lower than 0.05 and shown in the figure. In all charts, the error bar represents the standard deviation.

References

Abbasi, S., Sinha, S., Labit, E., Rosin, N.L., Yoon, G., Rahmani, W., Jaffer, A., Sharma, N., Hagner, A., Shah, P., Arora, R., Yoon, J., Islam, A., Uchida, A., Chang, C.K., Stratton, J.A., Scott, R.W., Rossi, F.M.V., Underhill, T.M., Biernaskie, J., 2020. Distinct Regulatory Programs Control the Latent Regenerative Potential of Dermal Fibroblasts during Wound Healing. Cell Stem Cell 27, 396-412.e6. https://doi.org/10.1016/j.stem.2020.07.008

Abd, E., Yousef, S.A., Pastore, M.N., Telaprolu, K., Mohammed, Y.H., Namjoshi, S., Grice, J.E., Roberts, M.S., 2016. Skin models for the testing of transdermal drugs. Clin Pharmacol 8, 163–176. https://doi.org/10.2147/CPAA.S64788

Abdellah, A.M., Khalil, M., Hamedelnie, E.I., Mustafa, M.H., 2019. Formulation and Evaluation of Hydrophilic Ointments Containing Dry Methanolic Extract of Acacia nilotica Pods. Asian Journal of Biological Sciences 12. https://doi.org/10.3923/ajbs.2019.583.588

Adams, T.S., Schupp, J.C., Poli, S., Ayaub, E.A., Neumark, N., Ahangari, F., Chu, S.G., Raby, B.A., Deluliis, G., Januszyk, M., Duan, Q., Arnett, H.A., Siddiqui, A., Washko, G.R., Homer, R., Yan, X., Rosas, I.O., Kaminski, N., 2020. Single-cell RNA-seq reveals ectopic and aberrant lung-resident cell populations in idiopathic pulmonary fibrosis. Science Advances 6, eaba1983. https://doi.org/10.1126/sciadv.aba1983

Arno, A.I., Amini-Nik, S., Blit, P.H., Al-Shehab, M., Belo, C., Herer, E., Jeschke, M.G., 2014. Effect of human Wharton's jelly mesenchymal stem cell paracrine signaling on keloid fibroblasts. Stem Cells Transl Med 3, 299–307. https://doi.org/10.5966/sctm.2013-0120

Ascensión, A.M., Fuertes-Álvarez, S., Ibañez-Solé, O., Izeta, A., Araúzo-Bravo, M.J., 2021. Human Dermal Fibroblast Subpopulations Are Conserved across Single-Cell RNA Sequencing Studies. J Invest Dermatol 141, 1735-1744.e35. https://doi.org/10.1016/j.jid.2020.11.028

Asparuhova, M.B., Kiryak, D., Eliezer, M., Mihov, D., Sculean, A., 2019. Activity of two hyaluronan preparations on primary human oral fibroblasts. Journal of Periodontal Research 54, 33–45. https://doi.org/10.1111/jre.12602

Bernstein, A.M., Twining, S.S., Warejcka, D.J., Tall, E., Masur, S.K., 2007. Urokinase Receptor Cleavage: A Crucial Step in Fibroblast-to-Myofibroblast Differentiation. MBoC 18, 2716–2727. https://doi.org/10.1091/mbc.e06-10-0912

Boateng, J.S., Matthews, K.H., Stevens, H.N.E., Eccleston, G.M., 2008. Wound Healing Dressings and Drug Delivery Systems: A Review. Journal of Pharmaceutical Sciences 97, 2892–2923. https://doi.org/10.1002/jps.21210

Brockes, J.P., Martin, P., Ferguson, M.W.J., O'Kane, S., 2004. Scar–free healing: from embryonic mechanisms to adult therapeutic intervention. Philosophical Transactions of the Royal Society of London. Series B: Biological Sciences 359, 839–850. https://doi.org/10.1098/rstb.2004.1475

Busco, G., Robert, E., Chettouh-Hammas, N., Pouvesle, J.-M., Grillon, C., 2020. The emerging potential of cold atmospheric plasma in skin biology. Free Radical Biology and Medicine 161, 290–304. https://doi.org/10.1016/j.freeradbiomed.2020.10.004

Cañedo-Dorantes, L., Cañedo-Ayala, M., 2019. Skin Acute Wound Healing: A Comprehensive Review. International Journal of Inflammation 2019, e3706315. https://doi.org/10.1155/2019/3706315

Cesarz, Z., Tamama, K., 2016. Spheroid Culture of Mesenchymal Stem Cells. Stem Cells Int 2016, 9176357. https://doi.org/10.1155/2016/9176357

Cho, S.S., Lee, J.H., Kim, K.M., Park, E.Y., Ku, S.K., Cho, I.J., Yang, J.H., Ki, S.H., 2021. REDD1 attenuates hepatic stellate cell activation and liver fibrosis via inhibiting of TGF-β/Smad signaling pathway. Free Radical Biology and Medicine 176, 246–256. https://doi.org/10.1016/j.freeradbiomed.2021.10.002

Cordeiro, J.V., Jacinto, A., 2013. The role of transcription-independent damage signals in the initiation of epithelial wound healing. Nat Rev Mol Cell Biol 14, 249–262. https://doi.org/10.1038/nrm3541

Correa-Gallegos, D., Jiang, D., Christ, S., Ramesh, P., Ye, H., Wannemacher, J., Kalgudde Gopal, S., Yu, Q., Aichler, M., Walch, A., Mirastschijski, U., Volz, T., Rinkevich, Y., 2019. Patch repair of deep wounds by mobilized fascia. Nature 576, 287–292. https://doi.org/10.1038/s41586-019-1794-y

Correa-Gallegos, D., Jiang, D., Rinkevich, Y., 2021. Fibroblasts as confederates of the immune system. Immunological Reviews 302, 147–162. https://doi.org/10.1111/imr.12972

Correa-Gallegos, D., Rinkevich, Y., 2022. Cutting into wound repair. The FEBS Journal 289, 5034–5048. https://doi.org/10.1111/febs.16078

Correa-Gallegos, D., Ye, H., Dasgupta, B., Sardogan, A., Kadri, S., Kandi, R., Dai, R., Lin, Y., Kopplin, R., Shenai, D.S., Wannemacher, J., Ichijo, R., Jiang, D., Strunz, M., Ansari, M., Angelidis, I., Schiller, H.B., Voltz, T., Machens, H.-G., Rinkevich, Y., 2023. CD201+ fascia progenitors choreograph injury repair. Nature 623, 792–802. https://doi.org/10.1038/s41586-023-06725-x

Davis, J., Salomonis, N., Ghearing, N., Lin, S.-C.J., Kwong, J.Q., Mohan, A., Swanson, M.S., Molkentin, J.D., 2015. MBNL1-mediated regulation of differentiation RNAs promotes myofibroblast transformation and the fibrotic response. Nat Commun 6, 10084. https://doi.org/10.1038/ncomms10084

Diegelmann, R.F., Evans, M.C., 2004. Wound healing: an overview of acute, fibrotic and delayed healing. Front Biosci 9, 283–289. https://doi.org/10.2741/1184

Driskell, R.R., Lichtenberger, B.M., Hoste, E., Kretzschmar, K., Simons, B.D., Charalambous, M., Ferron, S.R., Herault, Y., Pavlovic, G., Ferguson-Smith, A.C., Watt, F.M., 2013. Distinct fibroblast lineages determine dermal architecture in skin development and repair. Nature 504, 277–281. https://doi.org/10.1038/nature12783

Dunn, L., Prosser, H.C.G., Tan, J.T.M., Vanags, L.Z., Ng, M.K.C., Bursill, C.A., 2013. Murine model of wound healing. J Vis Exp e50265. https://doi.org/10.3791/50265

Duscher, D., Maan, Z.N., Whittam, A.J., Sorkin, M., Hu, M.S., Walmsley, G.G., Baker, H., Fischer, L.H., Januszyk, M., Wong, V.W., Gurtner, G.C., 2015. Fibroblast-Specific Deletion of Hypoxia Inducible Factor-1 Critically Impairs Murine Cutaneous Neovascularization and Wound Healing. Plast Reconstr Surg 136, 1004–1013. https://doi.org/10.1097/PRS.0000000000001699

Elias, P.M., Choi, E.H., 2005. Interactions among stratum corneum defensive functions. Exp Dermatol 14, 719–726. https://doi.org/10.1111/j.1600-0625.2005.00363.x

Eming, S.A., Martin, P., Tomic-Canic, M., 2014. Wound repair and regeneration: mechanisms, signaling, and translation. Sci Transl Med 6, 265sr6. https://doi.org/10.1126/scitranslmed.3009337

Farage, M.A., Miller, K.W., Elsner, P., Maibach, H.I., 2013. Characteristics of the Aging Skin. Adv Wound Care (New Rochelle) 2, 5–10. https://doi.org/10.1089/wound.2011.0356

Fischer, A., Correa-Gallegos, D., Wannemacher, J., Christ, S., Machens, H.-G., Rinkevich, Y., 2023. In vivo fluorescent labeling and tracking of extracellular matrix. Nat Protoc 18, 2876–2890. https://doi.org/10.1038/s41596-023-00867-y

Foster, D.S., Januszyk, M., Yost, K.E., Chinta, M.S., Gulati, G.S., Nguyen, A.T., Burcham, A.R., Salhotra, A., Ransom, R.C., Henn, D., Chen, K., Mascharak, S., Tolentino, K., Titan, A.L., Jones, R.E., da Silva, O., Leavitt, W.T., Marshall, C.D., des Jardins-Park, H.E., Hu, M.S., Wan, D.C., Wernig, G., Wagh, D., Coller, J., Norton, J.A., Gurtner, G.C., Newman, A.M., Chang, H.Y., Longaker, M.T., 2021. Integrated spatial multiomics reveals fibroblast fate during tissue repair. Proc Natl Acad Sci U S A 118, e2110025118. https://doi.org/10.1073/pnas.2110025118

Galiano, R.D., Michaels, J., Dobryansky, M., Levine, J.P., Gurtner, G.C., 2004. Quantitative and reproducible murine model of excisional wound healing. Wound Repair Regen 12, 485–492. https://doi.org/10.1111/j.1067-1927.2004.12404.x

Gifford, C.C., Lian, F., Tang, J., Costello, A., Goldschmeding, R., Samarakoon, R., Higgins, P.J., 2021. PAI-1 induction during kidney injury promotes fibrotic epithelial dysfunction via deregulation of klotho, p53, and TGF-β1-receptor signaling. FASEB J 35, e21725. https://doi.org/10.1096/fj.202002652RR

Grounds, M.D., Sorokin, L., White, J., 2005. Strength at the extracellular matrix-muscle interface. Scand J Med Sci Sports 15, 381–391. https://doi.org/10.1111/j.1600-0838.2005.00467.x

Gurtner, G.C., Werner, S., Barrandon, Y., Longaker, M.T., 2008. Wound repair and regeneration. Nature 453, 314–321. https://doi.org/10.1038/nature07039

Gushiken, L.F.S., Hussni, C.A., Bastos, J.K., Rozza, A.L., Beserra, F.P., Vieira, A.J., Padovani, C.R., Lemos, M., Junior, M.P., Silva, J.J.M. da, Nóbrega, R.H., Martinez, E.R.M., Pellizzon, C.H., 2017. Skin Wound Healing Potential and Mechanisms of the Hydroalcoholic Extract of Leaves and Oleoresin of*Copaifera langsdorffii*Desf. Kuntze in Rats. Evidence-Based Complementary and Alternative Medicine 2017. https://doi.org/10.1155/2017/6589270

Györfi, A.-H., Matei, A.-E., Fuchs, M., Liang, C., Rigau, A.R., Hong, X., Zhu, H., Luber, M., Bergmann, C., Dees, C., Ludolph, I., Horch, R.E., Distler, O., Wang, J., Bengsch, B., Schett, G., Kunz, M., Distler, J.H.W., 2021. Engrailed 1 coordinates cytoskeletal reorganization to induce myofibroblast differentiation. J Exp Med 218, e20201916. https://doi.org/10.1084/jem.20201916

Haro, M., Orsulic, S., 2018. A Paradoxical Correlation of Cancer-Associated Fibroblasts With Survival Outcomes in B-Cell Lymphomas and Carcinomas. Frontiers in Cell and Developmental Biology 6. https://doi.org/10.3389/fcell.2018.00098

Havrilak, J.A., Al-Shaer, L., Baban, N., Akinci, N., Layden, M.J., 2021. Characterization of the dynamics and variability of neuronal subtype responses during growth, degrowth, and regeneration of Nematostella vectensis. BMC Biology 19, 104. https://doi.org/10.1186/s12915-021-01038-9

Haydont, V., Neiveyans, V., Perez, P., Busson, É., Lataillade, J.-J., Asselineau, D., Fortunel, N.O., 2020. Fibroblasts from the Human Skin Dermo-Hypodermal Junction are Distinct from Dermal Papillary and Reticular Fibroblasts and from Mesenchymal Stem Cells and Exhibit a Specific Molecular Profile Related to Extracellular Matrix Organization and Modeling. Cells 9, 368. https://doi.org/10.3390/cells9020368

Hinz, B., 2007. Formation and function of the myofibroblast during tissue repair. J Invest Dermatol 127, 526–537. https://doi.org/10.1038/sj.jid.5700613

Hodge, J., Zamierowski, D.S., Robinson, J.L., Mellott, A.J., 2022. Evaluating polymeric biomaterials to improve next generation wound dressing design. Biomaterials Research 26. https://doi.org/10.1186/s40824-022-00291-5

Hogervorst, M., Rietveld, M., de Gruijl, F., El Ghalbzouri, A., 2018. A shift from papillary to reticular fibroblasts enables tumour–stroma interaction and invasion. Br J Cancer 118, 1089–1097. https://doi.org/10.1038/s41416-018-0024-y

Holick, M.F., 2007. Vitamin D Deficiency. N Engl J Med 357, 266–281. https://doi.org/10.1056/NEJMra070553

Hu, M.S., Borrelli, M.R., Lorenz, H.P., Longaker, M.T., Wan, D.C., 2018. Mesenchymal Stromal Cells and Cutaneous Wound Healing: A Comprehensive Review of the Background, Role, and Therapeutic Potential. Stem Cells International 2018. https://doi.org/10.1155/2018/6901983

Huang, T.T., Blackwell, S.J., Lewis, S.R., 1978. Ten years of experience in managing patients with burn contractures of axilla, elbow, wrist, and knee joints. Plast Reconstr Surg 61, 70–76. https://doi.org/10.1097/00006534-197801000-00012

Iimura, K., Watanabe, N., Masunaga, K., Miyazaki, S., Hotta, H., Kim, H., Hisajima, T., Takahashi, H., Kasuya, Y., 2016. Effects of a Gentle, Self-Administered Stimulation of Perineal Skin for Nocturia in Elderly Women: A Randomized, Placebo-Controlled, Double-Blind Crossover Trial. Plos One 11. https://doi.org/10.1371/journal.pone.0151726

Ito, M., Yang, Z., Andl, T., Cui, C., Kim, N., Millar, S.E., Cotsarelis, G., 2007. Wnt-dependent de novo hair follicle regeneration in adult mouse skin after wounding. Nature 447, 316–320. https://doi.org/10.1038/nature05766

Jiang, D., Christ, S., Correa-Gallegos, D., Ramesh, P., Kalgudde Gopal, S., Wannemacher, J., Mayr, C.H., Lupperger, V., Yu, Q., Ye, H., Mück-Häusl, M., Rajendran, V., Wan, L., Liu, J., Mirastschijski, U., Volz, T., Marr, C., Schiller, H.B., Rinkevich, Y., 2020. Injury triggers fascia fibroblast collective cell migration to drive scar formation through N-cadherin. Nat Commun 11, 5653. https://doi.org/10.1038/s41467-020-19425-1

Jiang, D., Correa-Gallegos, D., Christ, S., Stefanska, A., Liu, J., Ramesh, P., Rajendran, V., De Santis, M.M., Wagner, D.E., Rinkevich, Y., 2018. Two succeeding fibroblastic lineages drive dermal development and the transition from regeneration to scarring. Nat Cell Biol 20, 422–431. https://doi.org/10.1038/s41556-018-0073-8

Joost, S., Annusver, K., Jacob, T., Sun, X., Dalessandri, T., Sivan, U., Sequeira, I., Sandberg, R., Kasper, M., 2020. The Molecular Anatomy of Mouse Skin during Hair Growth and Rest. Cell Stem Cell 26, 441-457.e7. https://doi.org/10.1016/j.stem.2020.01.012

Jordana, M., Sarnstrand, B., Sime, P.J., Ramis, I., 1994. Immune-inflammatory functions of fibroblasts. European Respiratory Journal 7, 2212–2222. https://doi.org/10.1183/09031936.94.07122212

Judge, J.L., Owens, K.M., Pollock, S.J., Woeller, C.F., Thatcher, T.H., Williams, J.P., Phipps, R.P., Sime, P.J., Kottmann, R.M., 2015. Ionizing radiation induces myofibroblast differentiation via lactate dehydrogenase. American Journal of Physiology-Lung Cellular and Molecular Physiology 309, L879–L887. https://doi.org/10.1152/ajplung.00153.2015

Kao, C.-J., Chou, H.-Y., Lin, Y., Liu, Q., Wang, H.-M.D., 2019. Functional Analysis of Macromolecular Polysaccharides: Whitening, Moisturizing, Anti-Oxidant, and Cell Proliferation. Antioxidants 8. https://doi.org/10.3390/antiox8110533

Kim, S., Shin, Y., Choi, Y., Lim, K.M., Jeong, Y., Dayem, A.A., An, J., Song, K., Jang, S.B., Cho, S.-G., 2023. Improved Wound Healing and Skin Regeneration Ability of 3,2'-Dihydroxyflavone-Treated Mesenchymal Stem Cell-Derived Extracellular Vesicles. International Journal of Molecular Sciences 24. https://doi.org/10.3390/ijms24086964

Knapp, D., Tanaka, E.M., 2012. Regeneration and reprogramming. Current Opinion in Genetics & Development, Cell reprogramming 22, 485–493. https://doi.org/10.1016/j.gde.2012.09.006

Kollmannsberger, P., Bidan, C.M., Dunlop, J.W.C., Fratzl, P., Vogel, V., 2018. Tensile forces drive a reversible fibroblast-to-myofibroblast transition during tissue growth in engineered clefts. Science Advances 4. https://doi.org/10.1126/sciadv.aao4881

Krieg, T., Abraham, D., Lafyatis, R., 2007. Fibrosis in connective tissue disease: the role of the myofibroblast and fibroblast-epithelial cell interactions. Arthritis Research &Amp; Therapy 9. https://doi.org/10.1186/ar2188

Kuppe, C., Ibrahim, M.M., Kranz, J., Zhang, X., Ziegler, S., Perales-Patón, J., Jansen, J., Reimer, K.C., Smith, J.R., Dobie, R., Wilson-Kanamori, J.R., Halder, M., Xu, Y., Kabgani, N., Kaesler, N., Klaus, M., Gernhold, L., Puelles, V.G., Huber, T.B., Boor, P., Menzel, S., Hoogenboezem, R.M., Bindels, E.M.J., Steffens, J., Floege, J., Schneider, R.K., Saez-Rodriguez, J., Henderson, N.C., Kramann, R., 2021. Decoding myofibroblast origins in human kidney fibrosis. Nature 589, 281–286. https://doi.org/10.1038/s41586-020-2941-1

Leng, L., Ma, J., Lv, L., Wang, W., Gao, D., Zhu, Y., Wu, Z., 2020. Both Wnt signaling and epidermal stem cell-derived extracellular vesicles are involved in epidermal cell growth. Stem Cell Research &Amp; Therapy 11. https://doi.org/10.1186/s13287-020-01933-y

Li, J., Wang, J., Wang, Z., Xia, Y., Zhou, M., Zhong, A., Sun, J., 2020. Experimental models for cutaneous hypertrophic scar research. Wound Repair Regen 28, 126–144. https://doi.org/10.1111/wrr.12760

Li, R., Zeng, X., Han, Q., Lin, M., Long, L., Dan, H., Zhou, G., Chen, Q., 2014. Overexpression and Selectively Regulatory Roles of IL-23/IL-17 Axis in the Lesions of Oral Lichen Planus. Mediators of Inflammation 2014. https://doi.org/10.1155/2014/701094

Liu, J., Zhou, Z., Zhang, M., Song, F., Feng, C., Liu, H., 2022. Simple and robust 3D bioprinting of full-thickness human skin tissue. Bioengineered 13, 10090–10100. https://doi.org/10.1080/21655979.2022.2063651

Liu, X., Hu, H., Yin, J.Q., 2006. Therapeutic strategies against TGF-β signaling pathway in hepatic fibrosis. Liver International 26, 8–22. https://doi.org/10.1111/j.1478-3231.2005.01192.x

Luparello, C., Mauro, M., Lazzara, V., Vazzana, M., 2020. Collective Locomotion of Human Cells, Wound Healing and Their Control by Extracts and Isolated Compounds from Marine Invertebrates. Molecules 25. https://doi.org/10.3390/molecules25112471

M. G. Visha, Karunagaran, M., 2019. A review on wound healing. International Journal of Clinicopathological Correlation 3, 50–59.

Mapoung, S., Umsumarng, S., Semmarath, W., Arjsri, P., Thippraphan, P., Yodkeeree, S., Limtrakul, P., 2021. Skin Wound-Healing Potential of Polysaccharides from Medicinal

Mushroom Auricularia auricula-judae (Bull.). Journal of Fungi 7. https://doi.org/10.3390/jof7040247
Maquart, F.-X., Pickart, L., Laurent, M., Gillery, P., Monboisse, J.-C., Borel, J.-P., 1988. Stimulation of collagen synthesis in fibroblast cultures by the tripeptide-copper complex glycyl-L-histidyl-L-lysine-Cu2+. FEBS Letters 238, 343–346. https://doi.org/10.1016/0014-5793(88)80509-X
Massoz, L., Dupont, M.A., Manfroid, I., 2021. Zebra-Fishing for Regenerative Awakening in Mammals. Biomedicines 9, 65. https://doi.org/10.3390/biomedicines9010065
Masur, S.K., Dewal, H.S., Dinh, T.T., Erenburg, I., Petridou, S., 1996. Myofibroblasts differentiate from fibroblasts when plated at low density. Proceedings of the National Academy of Sciences 93, 4219–4223. https://doi.org/10.1073/pnas.93.9.4219
Mauroux, A., Joncour, P., Gillet, B., Hughes, S., Ardidie-Robouant, C., Marchand, L., Liabotis, A., Mailly, P., Monnot, C., Germain, S., Bordes, S., Closs, B., Ruggiero, F., Muller, L., 2020. Papillary and Reticular Fibroblasts Generate Distinct Microenvironments that Differentially Impact Angiogenesis. https://doi.org/10.1101/2020.11.29.402594
McCarty, S.M., Cochrane, C.A., Clegg, P.D., Percival, S.L., 2012. The role of endogenous and exogenous enzymes in chronic wounds: A focus on the implications of aberrant levels of both host and bacterial proteases in wound healing. Wound Repair and Regeneration 20, 125–136. https://doi.org/10.1111/j.1524-475X.2012.00763.x
McGrath, M.H., Hundahl, S.A., 1982. The spatial and temporal quantification of myofibroblasts. Plast Reconstr Surg 69, 975–985. https://doi.org/10.1097/00006534-198206000-00012
Meiners, S., Lloyd, C.M., Chambers, R.C., 2018. Cell–matrix interactions in lung disease and regeneration: ERS Lung Science Conference 2018 report. European Respiratory Review 27. https://doi.org/10.1183/16000617.0040-2018
Meyers, E., Kasliwal, N., Solorzano, B.R., Lai, E., Berry, A., Ganzer, P.D., Romero-Ortega, M.I., Rennaker, R.L., Kilgard, M.P., Hays, S.A., 2019. Enhancing plasticity in central networks improves motor and sensory recovery after nerve damage. Nature Communications 10. https://doi.org/10.1038/s41467-019-13695-0
Mohammed, B.M., Fisher, B.J., Kraskauskas, D., Ward, S., Wayne, J.S., Brophy, D.F., Fowler III, A.A., Yager, D.R., Natarajan, R., 2016. Vitamin C promotes wound healing through novel pleiotropic mechanisms. International Wound Journal 13, 572–584. https://doi.org/10.1111/iwj.12484
Muhammad, A.B., Pauzi, N.A.S., Arulselvan, P., Abas, F., Fakurazi, S., 2013. *In Vitro*Wound Healing Potential and Identification of Bioactive Compounds from*Moringa oleifera*Lam. BioMed Research International 2013. https://doi.org/10.1155/2013/974580
Myrna, K.E., Pot, S.A., Murphy, C.J., 2009. Meet the corneal myofibroblast: the role of myofibroblast transformation in corneal wound healing and pathology. Veterinary Ophthalmology 12, 25–27. https://doi.org/10.1111/j.1463-5224.2009.00742.x
Niu, C., Wang, L., Ji, D., Ren, M., Ke, D., Fu, Q., Zhang, K., Yang, X., 2022. Fabrication of SA/Gel/C scaffold with 3D bioprinting to generate micro-nano porosity structure for skin wound healing: a detailed animal in vivo study. Cell Regeneration 11. https://doi.org/10.1186/s13619-022-00113-y
Oh, S., Rho, N.-K., Byun, K.-A., Yang, J., Sun, H.J., Jang, M., Kang, D., Son, K.H., Byun, K., 2022. Combined Treatment of Monopolar and Bipolar Radiofrequency Increases Skin

Elasticity by Decreasing the Accumulation of Advanced Glycated End Products in Aged Animal Skin. International Journal of Molecular Sciences 23. https://doi.org/10.3390/ijms23062993
Ojeh, N., Pastar, I., Tomic-Canic, M., Stojadinovic, O., 2015. Stem Cells in Skin Regeneration, Wound Healing, and Their Clinical Applications. International Journal of Molecular Sciences 16. https://doi.org/10.3390/ijms161025476
Oliveira, R., Ferreira, J., Azevedo, L.F., Almeida, I.F., 2023. An Overview of Methods to Characterize Skin Type: Focus on Visual Rating Scales and Self-Report Instruments. Cosmetics 10, 14. https://doi.org/10.3390/cosmetics10010014
Pakshir, P., Noskovicova, N., Lodyga, M., Son, D.O., Schuster, R., Goodwin, A., Karvonen, H., Hinz, B., 2020. The myofibroblast at a glance. Journal of Cell Science 133, jcs227900. https://doi.org/10.1242/jcs.227900
Palmieri, T.L., Petuskey, K., Bagley, A., Takashiba, S., Greenhalgh, D.G., Rab, G.T., 2003. Alterations in functional movement after axillary burn scar contracture: a motion analysis study. J Burn Care Rehabil 24, 104–108. https://doi.org/10.1097/01.BCR.0000054170.62555.09
Panayi, A.C., Reitblat, C., Orgill, D.P., 2020. Wound Healing and Scarring, in: Ogawa, R. (Ed.), Total Scar Management: From Lasers to Surgery for Scars, Keloids, and Scar Contractures. Springer, Singapore, pp. 3–16. https://doi.org/10.1007/978-981-32-9791-3_1
Phan, Q.M., Sinha, S., Biernaskie, J., Driskell, R.R., 2021. Single-cell transcriptomic analysis of small and large wounds reveals the distinct spatial organization of regenerative fibroblasts. Exp Dermatol 30, 92–101. https://doi.org/10.1111/exd.14244
Potluri, T., Taylor, M., Stulberg, J.J., Lieber, R.L., Zhao, H., Bulun, S.E., 2022. An estrogen-sensitive fibroblast population drives abdominal muscle fibrosis in an inguinal hernia mouse model. JCI Insight 7. https://doi.org/10.1172/jci.insight.152011
Potter, D.A., Veitch, D., Johnston, G.A., 2019. Scarring and wound healing. Br J Hosp Med 80, C166–C171. https://doi.org/10.12968/hmed.2019.80.11.C166
Qarri, A., Rinkevich, B., 2023. Transient impacts of UV-B irradiation on whole body regeneration in a colonial urochordate. Dev Biol 503, 83–94. https://doi.org/10.1016/j.ydbio.2023.08.006
Ramesh, P., Ye, H., Dasgupta, B., Machens, H.-G., Rinkevich, Y., 2022. Visualizing Scar Development Using SCAD Assay - An Ex-situ Skin Scarring Assay. J Vis Exp. https://doi.org/10.3791/63808
Reddy, P.C., Gungi, A., Unni, M., 2019. Cellular and Molecular Mechanisms of Hydra Regeneration, in: Tworzydlo, W., Bilinski, S.M. (Eds.), Evo-Devo: Non-Model Species in Cell and Developmental Biology, Results and Problems in Cell Differentiation. Springer International Publishing, Cham, pp. 259–290. https://doi.org/10.1007/978-3-030-23459-1_12
Reinke, J.M., Sorg, H., 2012. Wound Repair and Regeneration. European Surgical Research 49, 35–43. https://doi.org/10.1159/000339613
Rinkevich, Y., Walmsley, G.G., Hu, M.S., Maan, Z.N., Newman, A.M., Drukker, M., Januszyk, M., Krampitz, G.W., Gurtner, G.C., Lorenz, H.P., Weissman, I.L., Longaker, M.T., 2015. Skin fibrosis. Identification and isolation of a dermal lineage with intrinsic fibrogenic potential. Science 348, aaa2151. https://doi.org/10.1126/science.aaa2151
Rouabhia, M., Park, H., Meng, S., Derbali, H., Zhang, Z., 2013. Electrical Stimulation Promotes Wound Healing by Enhancing Dermal Fibroblast Activity and Promoting

Myofibroblast Transdifferentiation. PLoS ONE 8. https://doi.org/10.1371/journal.pone.0071660

Ryu, J., Loza, C.A., Xu, H., Zhou, M., Hadley, J.T., Wu, J., You, H., Wang, H., Yang, J., Bai, J., Liu, F., Bialowas, C., Dong, L.Q., 2019. Potential Roles of Adiponectin Isoforms in Human Obesity with Delayed Wound Healing. Cells 8, 1134. https://doi.org/10.3390/cells8101134

Sagástegui-Guarniz, W.A., Silva-Correa, C.R., Torre, V.E.V.-L., González-Blas, M.V., Sagástegui-Guarniz, W.O., Calderón-Peña, A.A., Aspajo-Villalaz, C.L., Cruzado-Razco, J.L., Hilario-Vargas, J., 2021. Wound healing by topical application of Momordica charantia L. formulations on mice. Veterinary World. https://doi.org/10.14202/vetworld.2021.2699-2704

Saraswati, S., Marrow, S.M.W., Watch, L.A., Young, P.P., 2019. Identification of a pro-angiogenic functional role for FSP1-positive fibroblast subtype in wound healing. Nat Commun 10, 3027. https://doi.org/10.1038/s41467-019-10965-9

Sato, K., Asai, T.T., Jimi, S., 2020. Collagen-Derived Di-Peptide, Prolylhydroxyproline (Pro-Hyp): A New Low Molecular Weight Growth-Initiating Factor for Specific Fibroblasts Associated With Wound Healing. Frontiers in Cell and Developmental Biology 8.

Seifert, A.W., Kiama, S.G., Seifert, M.G., Goheen, J.R., Palmer, T.M., Maden, M., 2012. Skin shedding and tissue regeneration in African spiny mice (Acomys). Nature 489, 561–565. https://doi.org/10.1038/nature11499

Shao, H., Li, Y., Pastar, I., Xiao, M., Prokupets, R., Liu, S., Yu, K., Vazquez-Padron, R.I., Tomic-Canic, M., Velazquez, O.C., Liu, Z.-J., 2020. Notch1 signaling determines the plasticity and function of fibroblasts in diabetic wounds. Life Science Alliance 3. https://doi.org/10.26508/lsa.202000769

Shimazaki, T., 2016. Vertebrate Neural Stem Cells: Development, Plasticity, and Regeneration. The Keio Journal of Medicine 65, 1–15. https://doi.org/10.2302/kjm.2015-0005-IR

Shook, B.A., Wasko, R.R., Rivera-Gonzalez, G.C., Salazar-Gatzimas, E., López-Giráldez, F., Dash, B.C., Muñoz-Rojas, A.R., Aultman, K.D., Zwick, R.K., Lei, V., Arbiser, J.L., Miller-Jensen, K., Clark, D.A., Hsia, H.C., Horsley, V., 2018. Myofibroblast proliferation and heterogeneity are supported by macrophages during skin repair. Science 362, eaar2971. https://doi.org/10.1126/science.aar2971

Sim, P., Strudwick, X.L., Song, Y., Cowin, A.J., Garg, S., 2022. Influence of Acidic pH on Wound Healing In Vivo: A Novel Perspective for Wound Treatment. International Journal of Molecular Sciences 23. https://doi.org/10.3390/ijms232113655

Simon, L., Abdelmalek, B., 2012. Design of Skin Penetration Enhancers Using Replacement Methods for the Selection of the Molecular Descriptors. Pharmaceutics 4. https://doi.org/10.3390/pharmaceutics4030343

Sivaraj, D., Chen, K., Chattopadhyay, A., Henn, D., Wu, W., Noishiki, C., Magbual, N.J., Mittal, S., Mermin-Bunnell, A.M., Bonham, C.A., Trotsyuk, A.A., Barrera, J.A., Padmanabhan, J., Januszyk, M., Gurtner, G.C., 2021. Hydrogel Scaffolds to Deliver Cell Therapies for Wound Healing. Frontiers in Bioengineering and Biotechnology 9. https://doi.org/10.3389/fbioe.2021.660145

Škovranová, G., Čulenová, M., Treml, J., Dzurická, L., Marova, I., Sychrová, A., 2022. Prenylated phenolics from Morus alba against MRSA infections as a strategy for wound healing. Frontiers in Pharmacology 13.

Smith, P., 2018. Role of myofibroblasts in normal and pathological periodontal wound healing. Oral Diseases 24, 26–29. https://doi.org/10.1111/odi.12773

Srivastava, M., Mazza-Curll, K.L., van Wolfswinkel, J.C., Reddien, P.W., 2014. Whole-Body Acoel Regeneration Is Controlled by Wnt and Bmp-Admp Signaling. Current Biology 24, 1107–1113. https://doi.org/10.1016/j.cub.2014.03.042

Stunova, A., Vistejnova, L., 2018. Dermal fibroblasts-A heterogeneous population with regulatory function in wound healing. Cytokine Growth Factor Rev 39, 137–150. https://doi.org/10.1016/j.cytogfr.2018.01.003

Sullivan, J.V., Myers, S., 2022. 1 - Skin Structure and Function, Wound Healing and Scarring, in: Farhadieh, R.D., Bulstrode, N.W., Mehrara, B.J., Cugno, S. (Eds.), Plastic Surgery - Principles and Practice. Elsevier, pp. 1–14. https://doi.org/10.1016/B978-0-323-65381-7.00001-0

Tai, Y., Woods, E.L., Dally, J., Kong, D., Steadman, R., Moseley, R., Midgley, A.C., 2021. Myofibroblasts: Function, Formation, and Scope of Molecular Therapies for Skin Fibrosis. Biomolecules 11, 1095. https://doi.org/10.3390/biom11081095

Takeuchi, Y., Gotoh, N., 2023. Inflammatory cytokine-enriched microenvironment plays key roles in the development of breast cancers. Cancer Science 114. https://doi.org/10.1111/cas.15734

Tan, J.K.H., Watanabe, T., 2017. Stromal Cell Subsets Directing Neonatal Spleen Regeneration. Sci Rep 7, 40401. https://doi.org/10.1038/srep40401

Textor, J., Mandl, J.N., Boer, R.J. de, 2016. The Reticular Cell Network: A Robust Backbone for Immune Responses. PLOS Biology 14. https://doi.org/10.1371/journal.pbio.2000827

Uezumi, A., Nakatani, M., Ikemoto-Uezumi, M., Yamamoto, N., Morita, M., Yamaguchi, A., Yamada, H., Kasai, T., Masuda, S., Narita, A., Miyagoe-Suzuki, Y., Takeda, S., Fukada, S., Nishino, I., Tsuchida, K., 2016. Cell-Surface Protein Profiling Identifies Distinctive Markers of Progenitor Cells in Human Skeletal Muscle. Stem Cell Reports 7, 263–278. https://doi.org/10.1016/j.stemcr.2016.07.004

Velasquez, L.S., Sutherland, L.B., Liu, Z., Grinnell, F., Kamm, K.E., Schneider, J.W., Olson, E.N., Small, E.M., 2013. Activation of MRTF-A–dependent gene expression with a small molecule promotes myofibroblast differentiation and wound healing. Proceedings of the National Academy of Sciences 110, 16850–16855. https://doi.org/10.1073/pnas.1316764110

Wang, Y., Marshall, K.L., Baba, Y., Lumpkin, E.A., Gerling, G.J., 2015. Compressive Viscoelasticity of Freshly Excised Mouse Skin Is Dependent on Specimen Thickness, Strain Level and Rate. Plos One 10. https://doi.org/10.1371/journal.pone.0120897

Wolff, A., Hinman, V., 2021. The Use of Larval Sea Stars and Sea Urchins in the Discovery of Shared Mechanisms of Metazoan Whole-Body Regeneration. Genes 12, 1063. https://doi.org/10.3390/genes12071063

Woodley, D.T., 2017. Distinct Fibroblasts in the Papillary and Reticular Dermis: Implications for Wound Healing. Dermatol Clin 35, 95–100. https://doi.org/10.1016/j.det.2016.07.004

Wu, J., Fang, Z., Li, T., Hu, W., Wu, Y., Li, S., 2021. Maximizing the Utility of Transcriptomics Data in Inflammatory Skin Diseases. Frontiers in Immunology 12. https://doi.org/10.3389/fimmu.2021.761890

Wu, S., Rietveld, M., Hogervorst, M., de Gruijl, F., van der Burg, S., Vermeer, M., van Doorn, R., Welters, M., El Ghalbzouri, A., 2022. Human Papillary and Reticular Fibroblasts

Show Distinct Functions on Tumor Behavior in 3D-Organotypic Cultures Mimicking Melanoma and HNSCC. International Journal of Molecular Sciences 23, 11651. https://doi.org/10.3390/ijms231911651

Xiang, J., Zhou, L., Xie, Y., Zhu, Y., Xiao, L., Chen, Y., Chen, D., Wang, M., Cai, L., Guo, L., 2022. Mesh-like electrospun membrane loaded with atorvastatin facilitates cutaneous wound healing by promoting the paracrine function of mesenchymal stem cells. Stem Cell Research &Amp; Therapy 13. https://doi.org/10.1186/s13287-022-02865-5

Xiao, W., Tang, H., Wu, M., Liao, Y., Li, K., Li, L., Xu, X., 2017. Ozone oil promotes wound healing by increasing the migration of fibroblasts via PI3K/Akt/mTOR signaling pathway. Bioscience Reports 37, BSR20170658. https://doi.org/10.1042/BSR20170658

Xu, L.D., Xu, E.L., Li, L., 2018. Industry 4.0: state of the art and future trends. International Journal of Production Research 56, 2941–2962. https://doi.org/10.1080/00207543.2018.1444806

Xu, X., Chen, Bang, Zhu, S., Zhang, J., He, X., Cao, G., Chen, Bo, 2019. Hyperglycemia promotes Snail-induced epithelial–mesenchymal transition of gastric cancer via activating ENO1 expression. Cancer Cell Int 19, 344. https://doi.org/10.1186/s12935-019-1075-8

Yang, R., Su, B., 2010. Characterization and Comparison of the Tissue-Related Modules in Human and Mouse. PLoS ONE 5. https://doi.org/10.1371/journal.pone.0011730

You, X., Wu, J., Zhao, X., Jiang, X., Tao, W., Chen, Z., Huang, C., Zheng, T., Shen, X., 2021. Fibroblastic galectin-1-fostered invasion and metastasis are mediated by TGF-β1-induced epithelial-mesenchymal transition in gastric cancer. Aging (Albany NY) 13, 18464–18481. https://doi.org/10.18632/aging.203295

Yu, H., Wang, Y., Wang, D., Yi, Liu, Z., Wu, M., Wu, Y., Zhang, Q., 2022. Landscape of the epigenetic regulation in wound healing. Frontiers in Physiology 13. https://doi.org/10.3389/fphys.2022.949498

Zhang, X., Zheng, C., Gao, Z., Wang, L., Chen, C., Zheng, Y., Meng, Y., 2021. PKM2 promotes angiotensin-II-induced cardiac remodelling by activating TGF-β/Smad2/3 and Jak2/Stat3 pathways through oxidative stress. J Cell Mol Med 25, 10711–10723. https://doi.org/10.1111/jcmm.17007

Zhao, B., Guan, H., Liu, J.-Q., Zheng, Z., Zhou, Q., Zhang, J., Su, L.-L., Hu, D.-H., 2017. Hypoxia drives the transition of human dermal fibroblasts to a myofibroblast-like phenotype via the TGF-β1/Smad3 pathway. Int J Mol Med 39, 153–159. https://doi.org/10.3892/ijmm.2016.2816

List of Tables

Table 1: List of primers used for genotpying.....45

Table 2: List of Primary antibodies used 51

List of Figures

Figure 1 | RNA sequencing of stromal cells during wound healing reveals specialized states, a stepwise differentiation linked to wound healing phases 21

Figure 2 | CD201^{+} fascia fibroblasts undergo specialized differentiation during wound progression, exhibiting spatial and temporal patterns during this transition 23

Figure 3 | The manifestation of fibroblast markers in and PDPN^{CreER} x R26^{mTmG} double transgenic line 25

Figure 4 | Impairing the differentiation trajectory impairs the contraction capacity 27

Figure 5 | The RA gate promotes an inflammatory state and inhibits myofibroblast differentiation. 30

Figure 6 | RA fosters a tendency of hiring monocytes and cannot effectively facilitate further differentiation of fibroblasts. 33

Figure 7 | HIF1 facilitates the move to proto-myofibroblasts 34

Figure 8 | Inhibition of HIF1 limits progression of healing wounds 36

Figure 9 | Fibroblast differentiation in human skin diseases. 39

List of Publications

1. Ramesh, P., Ye, H., **Dasgupta, B**., Machens, H. G., Rinkevich, Y. Visualizing Scar Development Using SCAD Assay - An Ex-situ Skin Scarring Assay. J. Vis. Exp. (182), e63808, doi:10.3791/63808 (2022). PMID: 35575518.

2. Correa-Gallegos D*, Ye H*, **Dasgupta B***, Sardogan A, Kadri S, Kandi R, Dai R, Lin Y, Kopplin R, Shenai DS, Wannemacher J, Ichijo R, Jiang D, Strunz M, Ansari M, Angelidis I, Schiller HB, Voltz T, Machens HG, Rinkevich Y. CD201^{+} fascia progenitors choreograph injury repair. Nature. 2023 Nov;623(7988):792-802. doi: 10.1038/s41586-023-06725-x. Epub 2023 Nov 15. PMID: 37968392; PMCID: PMC10665192. ***Shared first author**

Contribution to the figures

In the presenting work, my contribution included:

Animal in-vivo experiments, ex-vivo cultures, histological preparation, fluorescence and multiphoton microscopy, image analysis, graph preparation and crucial assistance in figure generation and manuscript preparation. I performed extensive experiments both in-vivo and ex-vivo together with the conceptualization of multiple experimental procedures, leading to the decision of the shared first author status. More information can be found in the author's contribution to the paper.

In particular:

Figure 2 g-h, j: IF staining, image analysis and corresponding graph generation in $CD201^{creER}$ x $R26^{Ai14}$ mice with respective fibroblast markers of importance to show an abundance of specific populations in wound progression.

Figure 3 b-d: IF staining, image analysis and corresponding graph generation in $PDPN^{creER}$ x $R26^{mTmG}$ with respective fibroblast markers of importance to show an abundance of specific population in wound progression.

Figure 4 b-c, f: Ex-vivo experimentation of fascia contraction, bright field imaging, IF staining, image analysis and corresponding graph generation.

Figure 5 c-d, g-i: IF staining, ex-vivo experimentation, bright field imaging and quantification experiments to show the effects of different RA inducer isoforms on fascia contraction, co-localization image analysis and corresponding graph generation.

Figure 6 e-g: In vivo experimentation of RA agonist-treated excision wounds mice with regular bright field imaging of wound closure rate, Masson's trichrome staining and quantification and graph generation

Figure 7 b, f-i: IF staining showing the distribution of HIF1α at the indicated stage of wound healing. Ex-vivo experiments that show how HIF1α directs a shift in fibroblast to transit into the (proto)myofibroblast state. Further experiments in ex-vivo setup to show how classical signaling triggers like TGF ß and YAP activation are unable to rescue tissue contraction upon HIF1α inhibition: corresponding daily bright field imaging and extensive image analysis and graph preparation.

Figure 8 f, h-i: IF staining showing the blocking effects of HIF1α inhibitor injection at the indicated stage of wound healing and corresponding quantification. IF staining to show the various fibroblast marker distribution in correspondence to different fiber architecture. Imaging of control and HIF1α inhibitor treated wounds with the labelled matrix.

Acknowledgements

I would like to thank my direct supervisor Dr. Yuval Rinkevich for giving me the opportunity to perform research in the lab and to constantly motivate me to become a better individual in both science and as a human. This research work was funded by European Research Council Consolidator Grant (ERC-CoG 819933), the LEO Foundation (LF-OC-21-000835) and the European Foundation for the Study of Diabetes (EFSD) Anniversary Fund Program.

I would also like to thank every member of the Lung Health Immunity (LHI) group and all the other supporting departments and collaborators under the Helmholtz Munich umbrella. Special mention for Ejona Rusha from the Institute of Stem Cell Institute (ISF) for being there always to help and guide during scientific bottlenecks. My thankfulness to Dr. Sudharshan Padmarasu from the core facility of Genomics for helping me sequence all the single cell datasets.

I extend my heartfelt gratitude to my thesis committee, Prof. Dr. Jürgen Behr as my principal advisor and PD Dr. med. Anne Hilgendorff for being the external expert. My gratefulness to Prof. Dr. Ali Önder Yildrim and PD Dr. Claudia Staab-Weijnitz for providing guidance in the early times of my PhD research school career.

I thank the crew of IRBM both past and present Dr. Adrian Fischer, Dr. Martin Mück-Hausel, Dr. Safwen Kadri, Dr. Ryo Ichijo, Dr. Ravinder Kandi, Dr. Simon Christ, Dr. Vijayanand Rajendran, Dr. Pushkar Ramesh, Sandra Schiner, Ruiji Guo, Yue Lin, Ruoxuan Dai, George Vogelaar, Jiazheng Lai, Natalja Ring, Jin Xu, Shaoping Hu, Wei Han, Dr. Mahesh Gouda and Dr. Tankut Guney for the support and help during this journey. Separate mention to Christoph Deisenhofer, Asesh Chakraborty, Andy Qarri, Aydan Sardogan, Yiqun Su, Haifeng Ye, Xiangyu Zhang and Dr. Donovan Correa-Gallegos for being the cushion in the day-to-day life and the friends that were needed in the difficult times. Special thanks to Subhasree Dutta for being the lifeline, the smile behind all the bad days and constantly supporting and believing in me through thick and thin.

Beyond the lab, I want to thank my childhood friends Subhopriyo, Navoneel and Abhijit for being my friend and being the mentor, I sometimes needed and didn't want.

Finally, I want to thank my parents, my family and my cousins for providing that push every time I thought of stopping, supporting my dreams and believing in me.

I dedicate this thesis to all of you. Thank you.